EuroIntervention 2020;16:e913-e921 published online April 2020 ■ published online e-edition December 2020

Mini focus on bioresorbable scaffolds

Bioresorbable scaffolds versus permanent sirolimus-eluting stents in patients with ST-segment elevation myocardial infarction: vascular healing outcomes from the MAGSTEMI trial

Josep Gomez-Lara[1]*, MD, PhD; Luis Ortega-Paz[2], MD; Salvatore Brugaletta[2], MD, PhD; Javier Cuesta[3], MD; Sebastián Romaní[4], MD; Antonio Serra[5], MD; Pablo Salinas[6], MD; Bruno García del Blanco[7], MD; Javier Goicolea[8], MD; Rosana Hernández-Antolín[9], MD; Paula Antuña[3], MD; Rafael Romaguera[1], MD; Ander Regueiro[2], MD, PhD; Fernando Rivero[3], MD; Angel Cequier[1], MD, PhD; Fernando Alfonso[3], MD, PhD; Joan-Antoni Gomez-Hospital[1], MD, PhD; Manel Sabaté[2], MD, PhD

The authors' affiliations can be found in Appendix 1.

J. Gomez-Lara and L. Ortega-Paz contributed equally to this manuscript.

A list of study collaborators is included in Appendix 2.

This paper also includes supplementary data published online at: https://eurointervention.pcronline.com/doi/10.4244/EIJ-D-20-00198

KEYWORDS

- bioresorbable scaffolds
- optical coherence tomography
- STEMI

Abstract

Aims: The MAGSTEMI trial showed larger endothelium-independent vasodilatation with magnesium-based bioresorbable scaffolds (MgBRS) than with sirolimus-eluting stents (SES). However, restenosis was more frequent with MgBRS. The aims of this study were to compare the healing pattern between MgBRS and SES and to describe the main causes of restenosis, as assessed by optical coherence tomography (OCT).

Methods and results: Ninety-five consecutive patients from the randomised MAGSTEMI trial (MgBRS=48, SES=47) underwent OCT imaging at one year. Healing and bioresorption pattern were categorised into four groups: 1) indiscernible struts were observed in 33.3% versus 0% of patients (p<0.001); 2) struts integrated into the vessel wall in 22.9% versus 63.8% (p<0.001); 3) protruding struts in 37.5% versus 31.9% (p=0.568); and 4) protruding and malapposed struts in 6.3% versus 4.3% (p=0.663), respectively. MgBRS were not suitable for strut coverage analysis; SES presented with 5.6% uncovered struts. Scaffold discontinuities were observed in 10.4% and 0%, respectively (p=0.023). MgBRS presented smaller minimal lumen area (3.92±2.02 vs 6.31±1.71 mm²; p<0.001) and larger area stenosis (52.84±18.05 vs 25.02±14.58%; p<0.001). Scaffold measurements were only feasible in 50% of MgBRS, with the expansion index being smaller than in SES (0.58±0.16 vs 0.86±0.19; p<0.001). Scaffold collapse was observed in at least 50% of cases with MgBRS restenosis.

Conclusions: Both MgBRS and SES exhibited a low degree of neointima healing, but lumen dimensions were smaller with MgBRS at one year. Although the advanced bioresorption state of MgBRS hampers the assessment of scaffold collapse, this seems to be the main mechanism of restenosis. Future generations of MgBRS should increase and prolong the radial force. Clinical trial registration: NCT03234348

**Corresponding author: Heart Disease Institute, Hospital Universitari de Bellvitge, L'Hospitalet de Llobregat, c/ Feixa Llarga sn, 08907 Barcelona, Spain. E-mail: gomezjosep@hotmail.com*

SUBMITTED ON 17/02/2020 - REVISION RECEIVED ON 22/03/2020 - ACCEPTED ON 17/04/2020

DOI: 10.4244/EIJ-D-20-00198

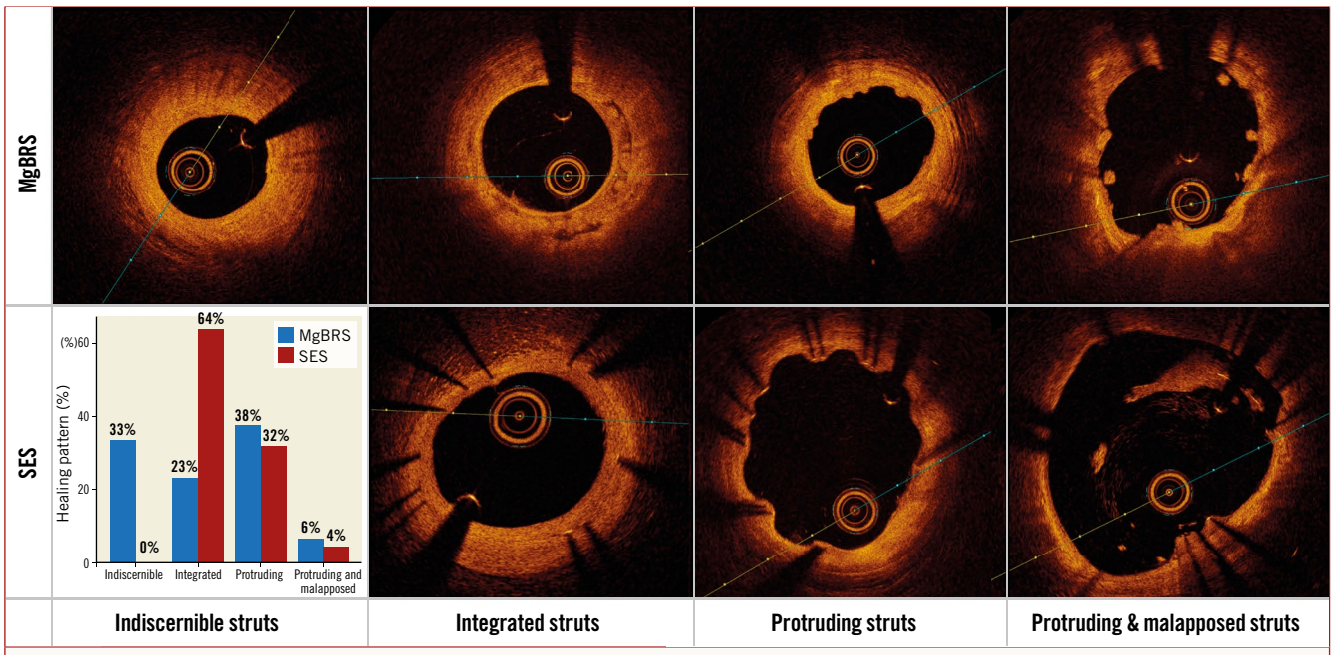

Visual summary. *Bioresorption and neointima patterns of Mg-based bioresorbabable scaffolds versus permanent sirolimus-eluting stents in STEMI patients at one year.*

Abbreviations

MgBRS	magnesium-based bioresorbable scaffold
OCT	optical coherence tomography
PPCI	primary percutaneous coronary intervention
SES	sirolimus-eluting stent
STEMI	ST-elevation myocardial infarction

Introduction

Primary percutaneous coronary intervention (PPCI) with stent implantation is the preferred reperfusion strategy in patients with ST-segment elevation myocardial infarction (STEMI). Stents implanted in the context of PPCI have been shown to exhibit greater malapposition and higher risk of stent thrombosis than stents implanted in other clinical scenarios[1,2]. Moreover, STEMI patients are often younger and present with softer plaque types as compared to other clinical settings. For these reasons, STEMI is theoretically one of the best targets for bioresorbable technology. Previous experience with polymeric poly-lactic acid-based bioresorbable scaffolds has shown that they are effective in STEMI patients[3-5].

The MAGSTEMI study (MAGnesium-based bioresorbable scaffold and vasomotor function in patients with acute ST-segment elevation myocardial infarction) is the first randomised study using the magnesium-based bioresorbable scaffold (MgBRS) (Magmaris®; Biotronik AG, Bülach, Switzerland). In this study, MgBRS showed greater endothelium-independent vasodilatation than a permanent metallic sirolimus-eluting stent (SES) (Orsiro; Biotronik AG) in STEMI patients at one-year follow-up[6]. However, MgBRS was associated with greater angiographic late lumen loss (0.61±0.55 mm vs 0.06±0.21 mm; p<0.001) and in-segment restenosis (20.0% vs 0%; p=0.001) than SES. The pathophysiologic mechanisms responsible for the greater lumen loss and restenosis rates in patients treated with MgBRS are still unknown.

The objectives of the present study are to describe and compare the main optical coherence tomography (OCT) parameters of stent healing between MgBRS and SES in STEMI patients at one year. This study also sought to investigate the mechanisms of angiographic in-segment MgBRS restenosis, as assessed by OCT.

Editorial, see page 869

Methods

POPULATION

The MAGSTEMI study (NCT03234348) is an investigator-initiated, multicentre, prospective and randomised clinical trial. This work was supported by the Spanish Heart Foundation. The design of the trial has been reported previously[7]. In summary, a total of 150 STEMI patients were randomised 1:1 to MgBRS or SES in 11 academic institutions. All patients were requested to undergo angiographic and vasomotor examination with nitroglycerine at one-year follow-up. The primary endpoint of the study was the observation of >3% vasodilatation within the scaffold segment[7]. The study was performed according to the provisions of the Declaration of Helsinki. The ethics committee of each participating centre approved the study protocol. Written informed consent was obtained from all patients.

The present investigation is a pre-specified substudy of the MAGSTEMI trial. As per protocol, three institutions (out of 11) of the MAGSTEMI trial were requested to perform OCT imaging during the one-year coronary angiography. This group of consecutive patients was classified as the "OCT per protocol group". Moreover, all study investigators aimed to perform OCT imaging in case of angiographic in-segment restenosis (diameter stenosis

≥50%) irrespective of the study institution. This group was classified as the "OCT per restenosis group".

OPTICAL COHERENCE TOMOGRAPHY

OCT imaging was performed after vasomotor examination with the Dragonfly™ OPTIS™ catheter (Abbott Vascular, Santa Clara, CA, USA) according to standard procedures. OCT analysis was performed by a dedicated core laboratory (BARCICORE-lab, Barcelona, Spain) using specific software for analysis (LightLab Imaging/Abbott Vascular). The analysed segment included the stent region and the stent margins defined as the vessel segment 5 mm proximal and distal to the stent.

Quantitative OCT analysis is described in **Supplementary Appendix 1**. Due to the advanced bioresorption state of the MgBRS, the scaffold area was clearly visible in only 40% of OCT cross-sections at one year. For this reason, all OCT variables involving scaffold measurements have been reported in patients with ≥40% of cross-sections suitable for scaffold area assessment. Stent expansion was calculated as minimal stent area/reference lumen area. Neointima area stenosis was calculated in all suitable cross-sections as neointima area/stent area *100.

Qualitative OCT analysis was performed by agreement of two analysts (J. Gomez-Lara and L. Ortega-Paz). According to the predominant number of cross-sections with one of the four different types of bioresorption and healing states, both study devices were classified into the following groups: 1) indiscernible struts, 2) visible struts completely integrated into the vessel wall; 3) visible struts protruding into the lumen causing a characteristic bumpy contour[8]; and 4) visible struts protruding and malapposed to the vessel wall. The core laboratory kappa value for this qualitative finding was 0.81. Other qualitative OCT findings are described in **Supplementary Appendix 2**. **Figure 1** and **Figure 2** show examples of different qualitative OCT findings. Scaffold restenosis types are described in **Supplementary Appendix 3**.

STATISTICAL ANALYSIS

Categorical variables are presented as counts and percentages, and continuous variables as mean±standard deviation (SD). Comparisons of categorical variables were estimated with the chi-square or Fisher's exact test as appropriate. Comparisons of continuous variables between groups were estimated with the Student's t-test. A two-sided p-value ≤0.05 was considered statistically significant. Statistical analysis was performed with SPSS software, version 20.0 (IBM Corp., Armonk, NY, USA).

Results

POPULATION

A total of 97 patients out of 108 included in the three OCT institutions underwent angiographic and OCT imaging at one year. According to the study flow chart **(Figure 3)**, 2 patients died before the scheduled angiography, 8 patients refused angiographic follow-up and 2 patients presented with acute stent thrombosis who were treated with thrombus aspiration and balloon dilatation.

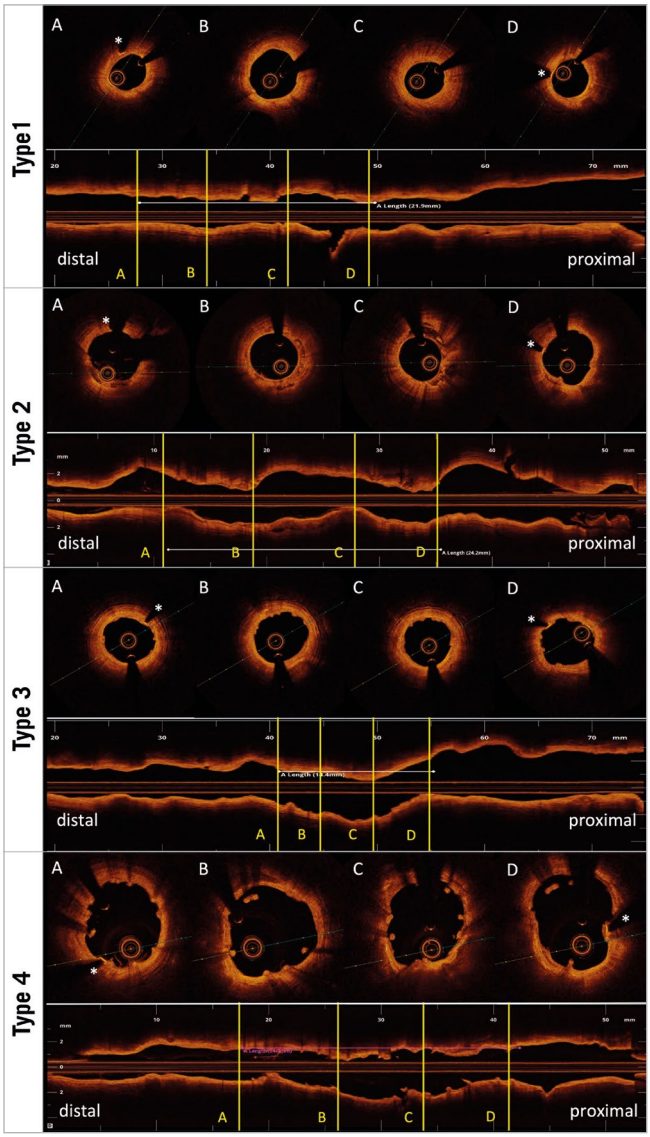

Figure 1. *Healing and bioresorption patterns of magnesium-based bioresorbable scaffolds. Type 1: indiscernible struts. Type 2: visible struts completely integrated into the vessel wall. Type 3: visible struts protruding into the lumen causing a characteristic bumpy contour. Type 4: visible struts protruding and malapposed to the vessel wall. * radiopaque markers.*

One of the patients with stent thrombosis also underwent scheduled 12-month angiography. Two patients were excluded due to suboptimal image quality (n=1) and the incapacity of the OCT catheter to cross the stent segment resulting in incomplete stent imaging (n=1). Therefore, a total of 95 patients were included in the present study (MgBRS=48 and SES=47) and were analysed in the "OCT per protocol group".

The MAGSTEMI trial had 14 patients with in-segment angiographic restenosis; all of them were included in the MgBRS arm[6]. Ten of these presented with angiographic restenosis and underwent OCT imaging as per protocol (in one of the three OCT institutions). These cases were already included in the "OCT per protocol group".

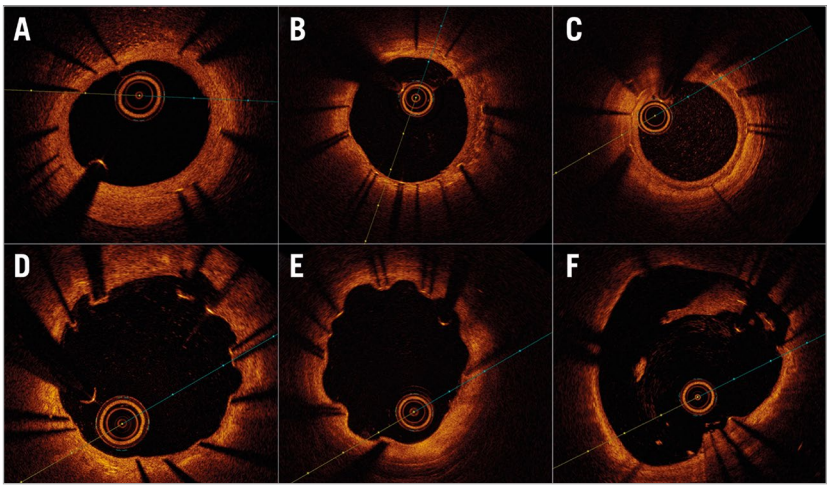

Figure 2. *Qualitative OCT findings of permanent metallic sirolimus-eluting stents. A) Homogeneous neointima pattern. B) Heterogeneous neointima pattern. C) Layered neointima pattern. D) RUTTS ≥30% (ratio of uncovered to total stent struts). E) Coronary evagination. F) Incomplete stent apposition.*

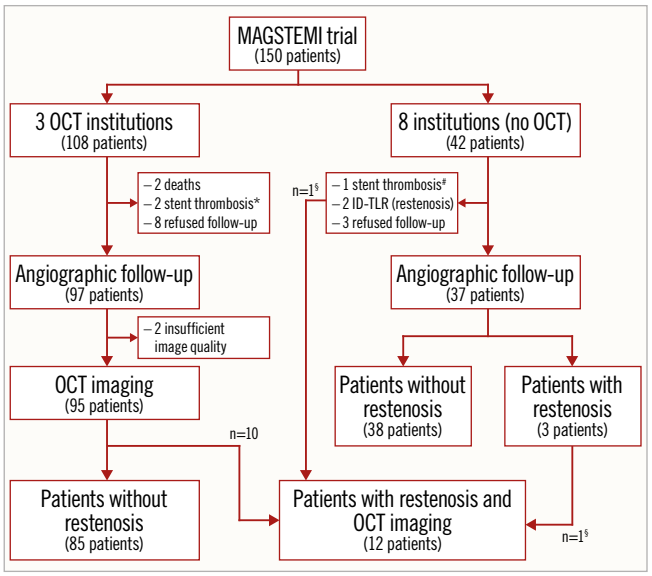

Figure 3. *Study flow chart. * One patient with acute stent thrombosis underwent one-year angiographic and OCT follow-up. # One patient with acute stent thrombosis underwent one-year angiographic follow-up. § Two patients with restenosis underwent OCT imaging in a study institution with no OCT protocol. ID-TLR: ischaemia-driven target lesion revascularisation.*

Moreover, two patients with in-segment restenosis included in two different institutions also underwent OCT imaging. Therefore, 12 out of 14 patients with MgBRS restenosis had OCT imaging. These 12 cases were analysed in the "OCT per restenosis group".

CLINICAL AND PROCEDURAL CHARACTERISTICS

The clinical, procedural and angiographic characteristics of patients included in the OCT per protocol group (n=97) were similar to those observed in patients without OCT (n=37). These data are shown in **Supplementary Table 1-Supplementary Table 3**.

The clinical characteristics of all patients included in the OCT per protocol group are shown in **Table 1**. There were no statistically significant differences between the MgBRS and SES arms. **Supplementary Table 4** shows the procedural characteristics of the OCT per protocol group. Procedural characteristics were similar between groups except for the percentage of post-dilatation, which was significantly higher in the MgBRS group (94.1% vs 16.7%; p=0.001).

Table 1. Baseline clinical characteristics.

	MgBRS N=50	SES N=47	*p*-value
Demographic data			
Age, years	59.2±10.5	59.5±9.6	0.883
Males, n (%)	42 (84.0)	43 (91.5)	0.263
Coronary risk factors, n (%)			
Current smoker	27 (54.0)	28 (59.6)	0.855
Diabetes mellitus	7 (14.0)	12 (25.5)	0.153
Insulin-dependent	2 (28.6)	1 (8.3)	0.523
Hypertension	24 (48.0)	19 (40.4)	0.453
Hypercholesterolaemia	34 (68.0)	25 (53.2)	0.135
Family history of coronary artery disease	7 (14.0)	2 (4.3)	0.098
Medical history, n (%)			
Previous myocardial infarction	5 (10.0)	2 (4.3)	0.275
Previous percutaneous coronary intervention	3 (6.0)	1 (2.1)	0.618
Chronic obstructive pulmonary disease	1 (2.0)	5 (10.6)	0.078

MgBRS: magnesium-based bioresorbable scaffold; SES: sirolimus-eluting stent

QUANTITATIVE CORONARY ANGIOGRAPHY ANALYSIS

The QCA characteristics of the OCT per protocol group are shown in **Table 2**. Baseline post-PCI results showed significantly smaller in-device minimal lumen diameter (2.50±0.30 vs 2.71±0.40 mm; p=0.005) and greater residual diameter stenosis (11.05±5.75 vs

Table 2. Quantitative coronary angiography analysis.

Index procedure		MgBRS N=50	SES N=47	*p*-value
Pre-PCI, mm				
MLD		0.19±0.36	0.19±0.38	0.981
%DS		93.14±12.82	92.87±13.70	0.959
Post PCI, mm				
In-stent	Length	19.71±4.62	18.40±6.33	0.250
	Mean LD	2.86±0.29	3.04±0.38	0.010
	MLD	2.50±0.30	2.71±0.40	0.005
	RVD	2.82±0.34	2.94±0.45	0.131
	%DS	11.05±5.75	7.83±4.78	0.024
In-segment	Length	29.26±4.90	27.95±6.40	0.263
	Mean LD	2.81±0.30	2.97±0.40	0.032
	MLD	2.11±0.38	2.27±0.43	0.056
	RVD	2.70±0.38	2.81±0.48	0.190
	%DS	21.57±9.16	19.14±9.87	0.146
In-stent lumen gain		2.31±0.48	2.52±0.60	0.034
In-segment lumen gain		1.92±0.53	2.08±0.61	0.182
Follow-up, mm				
In-stent	Length	19.87±4.86	18.44±6.30	0.052
	Mean LD	2.61±0.48	3.01±0.40	0.001
	MLD	1.94±0.57	2.65±0.45	0.001
	RVD	2.74±0.39	2.91±0.43	0.037
	%DS	29.63±17.32	9.16±7.18	0.001
In-segment	Length	29.49±5.19	28.04±6.35	0.220
	Mean LD	2.63±0.40	2.92±0.40	0.001
	MLD	1.78±0.49	2.25±0.44	0.001
	RVD	2.66±0.40	2.82±0.48	0.027
	%DS	32.87±15.66	19.66±8.77	0.001
Late lumen loss	In-stent LLL	0.56±0.47	0.06±0.25	0.001
	In-segment LLL	0.33±0.43	0.01±0.24	0.001
In-stent restenosis		10 (20.0)	0 (0.0)	0.001
In-segment restenosis		10 (20.0)	0 (0.0)	0.001

Data are presented as mean±standard deviation or n (%). DS: diameter stenosis; LLL: late lumen loss; Mean LD: mean lumen diameter; MgBRS: magnesium-based bioresorbable scaffold; MLD: minimal lumen diameter; PCI: percutaneous coronary intervention; RVD: reference vessel diameter; SES: sirolimus-eluting stent

Table 3. Qualitative OCT findings.

	MgBRS (n=48)	SES (n=47)	*p*-value
Healing pattern, n (%)			
Indiscernible struts (unclassified)	16 (33.3)	0	<0.001
Struts integrated into the vessel wall	11 (22.9)	30 (63.8)	<0.001
Struts protruding to the lumen	18 (37.5)	15 (31.9)	0.568
Struts protruding and malapposed	3 (6.3)	2 (4.3)	0.663
Neointima pattern, n (%)			
Absent or undetermined	21 (43.8)	16 (34.0)	0.066
Homogeneous	26 (54.1)	23 (48.9)	
Heterogeneous	1 (2.1)	2 (4.3)	
Layered	0	6 (12.8)	
Neoatherosclerosis, n (%)	1 (2.1)	4 (8.5)	0.161
Coronary evagination, n (%)	NA	35 (74.5)	NA
Major coronary evagination, n (%)	NA	20 (42.6)	NA
Uncovered struts, n (%)			
Patients with ≥5% uncovered struts	NA	18 (38.3)	NA
Patients with RUTTS ≥30%	NA	19 (40.4)	
Malapposed struts, n (%)			
Patients with ≥1 malapposed strut	18 (37.5)	21 (44.7)	0.477
Patients with ≥5% of malapposed struts	NA	7 (14.9)	NA
Strut discontinuities, n (%)	5 (10.4)	0	0.023
Plaque type behind the stent, n (%)			
Undetermined	3 (6.2)	3 (6.4)	0.532
Fibrotic	4 (8.3)	4 (8.5)	
Fibrolipidic	28 (58.3)	33 (70.2)	
Fibrocalcified	13 (27.1)	7 (14.9)	

MgBRS: magnesium-based bioresorbable scaffold; RUTTS: ratio of uncovered to total stent struts in 1 cross-section; SES: sirolimus-eluting stent

7.83±4.78%; p=0.024) with MgBRS than with SES. At one year, in-device late lumen loss was statistically significantly greater with MgBRS (0.56±0.47 mm) than with SES (0.06±0.25 mm), p=0.001.

OCT CHARACTERISTICS

Table 3 shows the qualitative OCT findings of the OCT per protocol group. The healing and bioresorption patterns between the devices were different in the two groups. Indiscernible struts were observed in 33.3% versus 0% of patients (p<0.001); visible struts completely integrated into the vessel wall were observed in 22.9% versus 63.8% (p<0.001); visible protruding struts were observed in 37.5% versus 31.9% (p=0.556); and visible protruding and malapposed struts were observed in 6.3% versus 4.3% (p=0.663), respectively. **Figure 4** shows a case treated with MgBRS presenting with complete bioresorption of the device at one year. Scaffold discontinuities were observed in 10.4% and 0% of patients (p=0.023), respectively.

Quantitative OCT findings are shown in **Table 4**. Strut coverage of MgBRS was not suitable for quantitative analysis. SES presented with 5.6% of uncovered struts and 2.0% of malapposed struts. Minimal lumen area was smaller (3.92±2.02 vs 6.31±1.71 mm²; p<0.001) and area stenosis was greater (52.84±18.05 vs 25.02±14.58%; p<0.001) with MgBRS than with SES. Scaffold measurements were only feasible in 50% of the MgBRS population, with the expansion index of the device being smaller than with SES (0.58±0.16 vs 0.86±0.19; p<0.001).

DESCRIPTION OF CASES WITH IN-SEGMENT MgBRS RESTENOSIS

A total of 14 patients presented with in-segment MgBRS restenosis in the MAGSTEMI trial[6]. A summary of the 14 cases is described in **Supplementary Table 5**. Only one case with MgBRS required unscheduled coronary angiography due to angina symptoms at nine months. The other 13 cases were asymptomatic and were observed

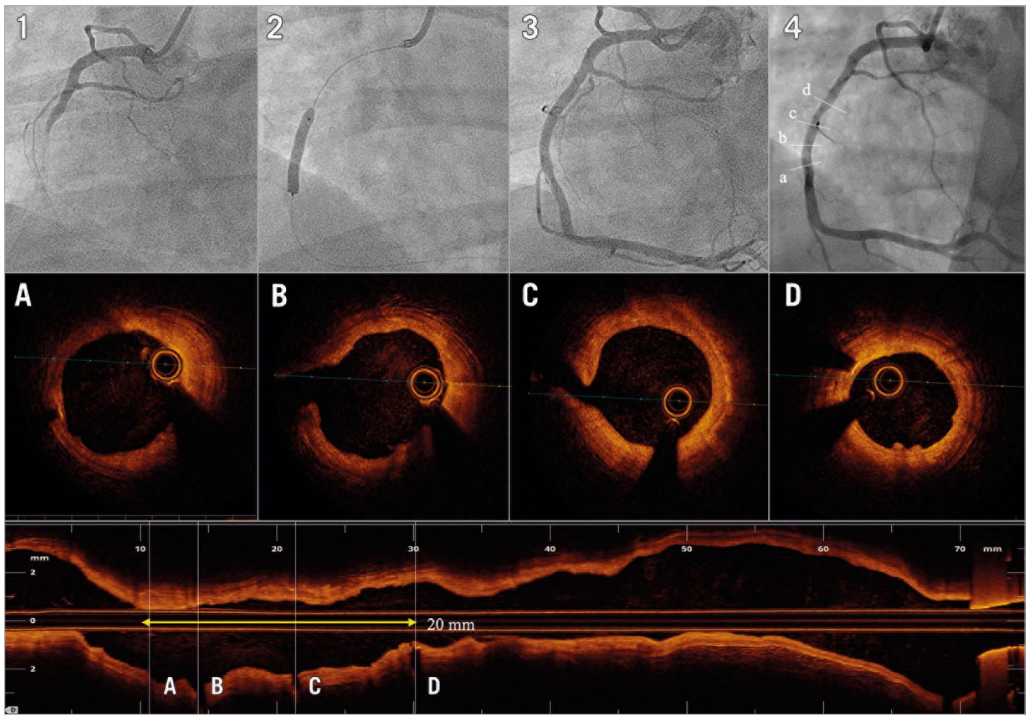

Figure 4. *Patient treated with MgBRS with complete bioresorption at one year. A 43-year-old male presented with inferior STEMI. Image 1 shows acute occlusion of the right coronary artery. After thrombus aspiration and predilatation, the patient was treated with a 3.5×20 mm MgBRS (image 2). Image 3 shows the final result after post-dilatation with a 3.5 non-compliant balloon. At 12 months, the patient underwent coronary angiography (image 4). Images A, B, C and D depict the one-year OCT imaging showing most of the cross-sections with indiscernible struts.*

Table 4. Quantitative OCT findings.

		MgBRS (n=48) (struts=NA)	SES (n=47) (struts=10,530)	*p*-value
Lesion-level analysis				
Reference lumen area, mm²		8.16±2.46	8.60±2.70	0.416
Device length, mm		20.75±5.22	21.64±7.75	0.510
Lumen area, mm²	Minimal	3.92±2.02	6.31±1.71	<0.001
	Mean	6.60±2.30	7.75±1.97	0.010
Stent area, mm²*	Minimal	4.77±1.65	7.11±1.59	<0.001
	Mean	6.95±2.17	8.27±1.80	0.009
Scaffold expansion index		0.58±0.16	0.86±0.19	<0.001
Mean malapposition area, mm²*		0.10±0.18	0.11±0.29	0.883
Mean neointima area, mm²*		0.75±0.32	0.65±0.55	0.422
Neointima area stenosis, %*	Mean	13.76±8.83	8.35±6.74	0.006
	Maximal	27.20±12.91	18.58±10.25	0.003
In-device area stenosis, %		52.84±18.05	25.02±14.58	<0.001
Strut-level analysis				
Uncovered struts, n (%)		NA	593 (5.6)	NA
Malapposed struts, n (%)		NA	209 (2.0)	NA
Uncovered & malapposed struts, n (%)		NA	166 (1.6)	NA
Mean neointima thickness, µm		NA	80.8±82.1	NA

* Scaffold, malapposition and neointima area measurements were performed in 24 MgBRS patients suitable for scaffold area assessment (≥40% of OCT cross-sections in each patient). MgBRS: magnesium-based bioresorbable scaffold; SD: standard deviation; SES: sirolimus-eluting stent

during the 12-month scheduled, per protocol, coronary angiography. Twelve out of 14 cases with MgBRS restenosis had OCT imaging and were included in the "OCT per restenosis group". These cases are shown in **Supplementary Figure 1-Supplementary Figure 12**. According to the OCT qualitative analysis, scaffold collapse (n=5; 42%) was the main cause of scaffold failure. There were 3 cases (25%) with unknown causes due to the advanced bioresorption state of the scaffold at one year, and 2 cases (17%) were attributed to excessive neointima tissue (1 case [8%] had a combination of scaffold collapse and excessive neointima tissue and 1 case [8%] was attributed to scaffold discontinuity).

Discussion

The main findings of the present study are: 1) remnant struts were observed in 70% of patients treated with MgBRS at one year; 2) both MgBRS and SES exhibited a low degree of neointima since >35% of patients presented with protruding or protruding and malapposed struts as the most predominant healing patterns; 3) patients treated with MgBRS had smaller lumen dimensions and greater area stenosis than patients treated with SES at one-year follow-up; and 4) according to observations performed in 40% of OCT cross-sections with remnant scaffold struts, scaffold collapse seemed to be the main mechanism of scaffold restenosis.

The randomised MAGSTEMI study is the first head-to-head comparison of MgBRS versus the gold standard permanent

metallic stent. The first generation of MgBRS (AMS®; Biotronik) had thick struts (165 µm) and no drug elution. The first-in-man investigation using this iteration reported 47.5% angiographic restenosis that was mainly attributed to scaffold recoil and excessive neointima response[9]. The second generation of the MgBRS scaffold (DREAMS®; Biotronik) was aimed at prolonging the radial force and inhibiting neointima formation by reducing the strut thickness (120 µm), coating the strut surface with bioresorbable polymer (poly lactic-co-glycolic acid) and coating the scaffold with an antiproliferative drug (paclitaxel). The first-in-man study using this iteration also showed a remarkable lumen loss (0.65±0.50 mm) and restenosis rate (17%) at six months. According to IVUS, lumen loss was mainly driven by scaffold recoil (73%)[10]. The third and current generation of MgBRS (DREAMS-2 or Magmaris; Biotronik) aimed to prevent scaffold recoil by enlarging the strut thickness (150 µm) and coating the scaffold with more stable polymer (poly-lactic acid). This iteration, coated with sirolimus, was evaluated in the first-in-man BIOSOLVE-II trial[11]. In this study, angiographic results were acceptable (lumen loss of 0.44±0.36 mm and 5% restenosis), and IVUS did not show relevant scaffold recoil at six months[11].

However, an OCT substudy of the BIOSOLVE-II trial showed that patients treated with overexpanded devices (expansion index >1.0 at the end of the baseline procedure) presented with greater lumen loss than patients treated without overexpansion. The authors hypothesised that excessive overexpansion during implantation could provoke polymer fractures which could induce premature degradation of the magnesium alloy and an early loss of the radial force[12]. In the present study, patients presenting with greater lumen loss (>0.50 mm) at one year had a smaller baseline reference vessel diameter (RVD) (2.73 mm vs 2.92 mm; p=0.07) and were treated using a higher balloon to artery ratio (1.18 vs 1.12; p=0.08) than patients with less angiographic lumen loss (≤0.5 mm). Therefore, scaffold overexpansion was also probably related to in-scaffold restenosis.

On the other hand, the BIOSOLVE-II study included patients with stable coronary artery disease. In contrast, the MAGSTEMI trial only included patients with STEMI. It is plausible that inflamed coronary plaques, such as culprit STEMI plaques, may also speed the degradation of the scaffold polymer which could facilitate scaffold recoil. In a series of cases with clinically driven MgBRS restenosis, scaffold collapse was identified as the main cause of scaffold failure (58%), as assessed by OCT; five out of seven cases with scaffold collapse were implanted in the setting of STEMI[13]. In the present study, scaffold collapse was identified in 50% of cases with angiographic restenosis. However, there were also three (25%) patients with in-scaffold restenosis who presented with indiscernible struts, classified as unknown mechanism, in whom scaffold collapse cannot be discounted.

Scaffold failure mechanisms seem different between different types of bioresorbable scaffold (BRS). Scaffold discontinuities were attributed as being the main cause of scaffold failure using polymer-based BRS (Absorb™; Abbott Vascular)[14]. In event-free STEMI patients treated with polymeric BRS, strut discontinuities were observed in 26% at three years[15]. In the present study, only 10% of cases presented with scaffold discontinuities. Moreover, in a series of cases with MgBRS failure, only 33% were attributed to fractures; all of those cases presented as stable or unstable angina syndromes without angiographic signs of scaffold thrombosis[13]. This reinforces the hypothesis that MgBRS have lower thrombogenicity and may have a lower percentage of scaffold thrombosis than polymeric BRS, even in cases with strut discontinuities. In a swine arteriovenous shunt model including permanent SES, MgBRS and polymer-based BRS, MgBRS showed less platelet coverage (3.0%) than SES (4.6%) and polymer-based BRS (21.8%)[16].

Limitations

The present study has several limitations. First, the bioresorption state of MgBRS, as assessed by OCT, hampers the quantification of some of the study findings. For example, scaffold collapse assessment has been based on only 40% of OCT cross-sections suitable for scaffold area measurement. It is uncertain if the other cases would have shown similar results. Second, the healing and bioresorption pattern is often heterogeneous showing contiguous regions with remnant and indiscernible struts. The qualitative patterns used in the present investigation represent the most common healing pattern throughout the scaffold. Third, due to the nature of the study, which included acute patients in the setting of PPCI procedures, there was no OCT imaging during the implantation. Serial assessment of OCT images between baseline and one year would allow better assessment of the healing pattern and scaffold recoil. Finally, the MAGSTEMI trial included <5% of all STEMI patients undergoing PPCI during the study recruitment; this is indicative of a selected group of patients not representative of the all-comer population.

Conclusions

At one year, both MgBRS and SES exhibited a low degree of neointima healing. However, MgBRS had smaller lumen dimensions and greater diameter stenosis than SES. Although the advanced bioresorption state of MgBRS hampers the assessment of scaffold dimensions, the analysis of patients with remnant scaffold struts indicated a low expansion index and suggests scaffold recoil as the most plausible cause of lumen loss. Moreover, scaffold collapse was observed in at least 50% of cases with angiographic restenosis. Future generations of MgBRS should increase the radial force and prolong the scaffolding time of the device.

Impact on daily practice

The current generation of the magnesium-based bioresorbable scaffold (MgBRS) shows a high percentage of angiographic restenosis in STEMI patients. According to the present study, the most plausible explanation for this is scaffold collapse. New generations of MgBRS should increase and prolong the radial force of the device and test its efficacy in powered randomised trials with imaging substudies.

Appendix 1. Authors' affiliations

1. Hospital Universitari de Bellvitge, Institut d'Investigació Biomèdica de Bellvitge (IDIBELL), L'Hospitalet de Llobregat, Barcelona, Spain; 2. Hospital Clínic i Provincial de Barcelona, IDIBAPS (Institut d'Investigacions Biomèdiques August Pi i Sunyer), Barcelona, Spain; 3. Hospital Universitario La Princesa, Instituto Investigación Sanitaria-IP, Madrid, Spain; 4. Hospital San Pedro de Alcántara, Cáceres, Spain; 5. Hospital Universitari de Sant Pau, Barcelona, Spain; 6. Hospital Clínico San Carlos, Instituto de Investigación Sanitaria del Hospital Clínico San Carlos (IdISSC), Madrid, Spain; 7. Hospital Universitari Vall d'Hebrón, Barcelona, Spain; 8. Hospital Puerta de Hierro-Majadahonda, Madrid, Spain; 9. Hospital Ramón y Cajal, Madrid, Spain.

Appendix 2. Study collaborators

Xavier Freixa, MD, PhD; *Hospital Clínic i Provincial de Barcelona, IDIBAPS (Institut d'Investigacions Biomèdiques August Pi i Sunyer), Barcelona, Spain*. Monica Masotti, MD, PhD; *Hospital Clínic i Provincial de Barcelona, IDIBAPS (Institut d'Investigacions Biomèdiques August Pi i Sunyer), Barcelona, Spain*. Jose Luís Ferreiro, MD; *Hospital Universitari de Bellvitge, Institut d'Investigació Biomèdica de Bellvitge (IDIBELL), Universitat de Barcelona, L'Hospitalet de Llobregat, Spain*. Gerard Roura, MD, PhD; *Hospital Universitari de Bellvitge, Institut d'Investigació Biomèdica de Bellvitge (IDIBELL), Universitat de Barcelona, L'Hospitalet de Llobregat, Spain*. Teresa Bastante, MD; *Hospital Universtiario La Princesa, Instituto de Investigación Sanitaria-IP, Madrid, Spain*. Marcelo Jiménez, MD; *Hospital Universitari de Sant Pau, Barcelona, Spain*. Imanol Otaegui, MD; *Hospital Universitari Vall d'Hebrón, Barcelona, Spain*. Pascual Bordes, MD; *Hospital General de Alicante, Alicante, Spain*. Andres Iñiguez, MD; *Hospital Alvaro Cunqueiro, Vigo, Spain*.

Funding

This work was supported by the Spanish Heart Foundation.

Conflict of interest statement

J. Gómez-Lara and L. Ortega-Paz have received fees from BARCICORE-lab. M. Sabaté is a consultant for Abbott Vascular and iVascular (not related to the present study). A. Cequier has received grants and personal fees from Abbott Vascular, Medtronic, Boston Scientific, and Biosensors (not related to the present study). P. Salinas has received speaker fees from Terumo, Boston Scientific, AlviMedica and Biomenco (not related to the present study). S. Brugaletta is a consultant for Boston Scientific and iVascular and has received a research grant to his institution from AstraZeneca (not related to the present study). A. Regueiro has received speaker fees from Abbott and Cardinal Health (not related to the present study). The other authors/study collaborators have no conflicts of interest to declare.

References

1. Gomez-Lara J, Salvatella N, Gonzalo N, Hernandez-Hernandez F, Fernandez-Nofrerias E, Sanchez-Recalde A, Bastante T, Marcano A, Romaguera R, Ferreiro JL, Roura G, Teruel L, Ariza-Solé A, Miranda-Guardiola F, Rodriguez Garcia-Abad V, Gomez-Hospital JA, Alfonso F, Cequier A. IVUS-guided treatment strategies for definite late and very late stent thrombosis. *EuroIntervention.* 2016;12:e1355-65.

2. Gonzalo N, Barlis P, Serruys PW, Garcia-Garcia HM, Onuma Y, Ligthart J, Regar E. Incomplete stent apposition and delayed tissue coverage are more frequent in drug-eluting stents implanted during primary percutaneous coronary intervention for ST-segment elevation myocardial infarction than in drug-eluting stents implanted for stable/unstable angina: insights from optical coherence tomography. *JACC Cardiovasc Interv.* 2009;2:445-52.

3. Sabaté M, Windecker S, Iniguez A, Okkels-Jensen L, Cequier A, Brugaletta S, Hofma SH, Räber L, Christiansen EH, Suttorp M, Pilgrim T, Anne van Es G, Sotomi Y, Garcia-Garcia HM, Onuma Y, Serruys PW. Everolimus-eluting bioresorbable stent vs. durable polymer everolimus-eluting metallic stent in patients with ST-segment elevation myocardial infarction: results of the randomized ABSORB ST-segment elevation myocardial infarction-TROFI II trial. *Eur Heart J.* 2016;37:229-40.

4. Byrne RA, Alfonso F, Schneider S, Maeng M, Wiebe J, Kretov E, Bradaric C, Rai H, Cuesta J, Rivero F, Hoppmann P, Schlichtenmaier J, Christiansen EH, Cassese S, Joner M, Schunkert H, Laugwitz KL, Kastrati A. Prospective, randomized trial of bioresorbable scaffolds vs. everolimus-eluting stents in patients undergoing coronary stenting for myocardial infarction: the Intracoronary Scaffold Assessment a Randomized evaluation of Absorb in Myocardial Infarction (ISAR-Absorb MI) trial. *Eur Heart J.* 2019;40:167-76.

5. Brugaletta S, Gori T, Low AF, Tousek P, Pinar E, Gomez-Lara J, Ortega-Paz L, Schulz E, Chan MY, Kocka V, Hurtado J, Gomez-Hospital JA, Giacchi G, Munzel T, Lee CH, Cequier A, Valdes M, Widimsky P, Serruys PW, Sabaté M. ABSORB bioresorbable vascular scaffold vs. everolimus-eluting metallic stent in ST-segment elevation myocardial infarction (BVS EXAMINATION study): 2-Year results from a propensity score matched comparison. *Int J Cardiol.* 2016;214:483-4.

6. Sabaté M, Alfonso F, Cequier A, Romani S, Bordes P, Serra A, Iniguez A, Salinas P, Garcia Del Blanco B, Goicolea J, Hernandez-Antolin R, Cuesta J, Gomez-Hospital JA, Ortega-Paz L, Gomez-Lara J, Brugaletta S. Magnesium-Based Resorbable Scaffold versus Permanent Metallic Sirolimus-Eluting Stent in Patients with ST-Segment Elevation Myocardial Infarction: The MAGSTEMI Randomized Clinical Trial. *Circulation.* 2019;140:1904-16.

7. Brugaletta S, Cequier A, Alfonso F, Iniguez A, Romani S, Serra A, Salinas P, Goicolea J, Bordes P, Del Blanco BG, Hernandez-Antolin R, Pernigotti A, Gomez-Lara J, Sabaté M. MAGnesium-based bioresorbable scaffold and vasomotor function in patients with acute ST segment elevation myocardial infarction: The MAGSTEMI trial: Rationale and design. *Catheter Cardiovasc Interv.* 2019;93:64-70.

8. Alfonso F, Cuesta J, Garcia-Guimaraes M, Rivero F. "Bumpy" neointima: the fingerprint of bioabsorbable magnesium scaffold resorption. *EuroIntervention.* 2019;15:e380-1.

9. Erbel R, Di Mario C, Bartunek J, Bonnier J, de Bruyne B, Eberli FR, Erne P, Haude M, Heublein B, Horrigan M, Ilsley C, Böse D, Koolen J, Lüscher TF, Weissman N, Waksman R; PROGRESS-AMS (Clinical Performance and Angiographic Results of Coronary Stenting with Absorbable Metal Stents) Investigators. Temporary scaffolding of coronary arteries with bioabsorbable magnesium stents: a prospective, non-randomised multicentre trial. *Lancet.* 2007;369:1869-75.

10. Haude M, Erbel R, Erne P, Verheye S, Degen H, Böse D, Vermeersch P, Wijnbergen I, Weissman N, Prati F, Waksman R, Koolen J. Safety and performance of the drug-eluting absorbable metal scaffold (DREAMS) in patients with de-novo coronary lesions: 12 month results of the prospective, multicentre, first-in-man BIOSOLVE-I trial. *Lancet.* 2013;381:836-44.

11. Haude M, Ince H, Abizaid A, Toelg R, Lemos PA, von Birgelen C, Christiansen EH, Wijns W, Neumann FJ, Kaiser C, Eeckhout E, Lim ST, Escaned J, Garcia-Garcia HM, Waksman R. Safety and performance of the

second-generation drug-eluting absorbable metal scaffold in patients with de-novo coronary artery lesions (BIOSOLVE-II): 6 month results of a prospective, multicentre, non-randomised, first-in-man trial. *Lancet.* 2016; 387:31-9.

12. Ozaki Y, Garcia-Garcia HM, Hideo-Kajita A, Kuku KO, Haude M, Ince H, Abizaid A, Tölg R, Lemos PA, von Birgelen C, Christiansen EH, Wijns W, Escaned J, Dijkstra J, Waksman R. Impact of procedural characteristics on coronary vessel wall healing following implantation of second-generation drug-eluting absorbable metal scaffold in patients with de novo coronary artery lesions: an optical coherence tomography analysis. *Eur Heart J Cardiovasc Imaging.* 2019;20:916-24.

13. Ortega-Paz L, Brugaletta S, Gomez-Lara J, Sanchis J, Fernandez-Diaz JA, Artaiz-Urdaci M, Alfonso F, Garcia-Garcia HM, Sabaté M. Second-generation drug-eluting absorbable metal scaffold target-lesion revascularization: an optical coherence tomography case series study and literature review. *EuroIntervention.* 2019 Sep 3. [Epub ahead of print].

14. Yamaji K, Ueki Y, Souteyrand G, Daemen J, Wiebe J, Nef H, Adriaenssens T, Loh JP, Lattuca B, Wykrzykowska JJ, Gomez-Lara J, Timmers L, Motreff P, Hoppmann P, Abdel-Wahab M, Byrne RA, Meincke F, Boeder N, Honton B, O'Sullivan CJ, Ielasi A, Delarche N, Christ G, Lee JKT, Lee M, Amabile N, Karagiannis A, Windecker S, Räber L. Mechanisms of Very Late Bioresorbable Scaffold Thrombosis: The INVEST Registry. *J Am Coll Cardiol.* 2017;70: 2330-44.

15. Gomez-Lara J, Brugaletta S, Ortega-Paz L, Vandeloo B, Moscarella E, Salas M, Romaguera R, Roura G, Ferreiro JL, Teruel L, Gracida M, Windecker S, Serruys PW, Gomez-Hospital JA, Sabaté M, Cequier A. Long-Term Coronary Functional Assessment of the Infarct-Related Artery Treated With Everolimus-Eluting Bioresorbable Scaffolds or Everolimus-Eluting Metallic Stents: Insights of the TROFI II Trial. *JACC Cardiovasc Interv.* 2018;11:1559-71.

16. Waksman R, Lipinski MJ, Acampado E, Cheng Q, Adams L, Torii S, Gai J, Torguson R, Hellinga DM, Westman PC, Joner M, Zumstein P, Kolodgie FD, Virmani R. Comparison of Acute Thrombogenicity for Metallic and Polymeric Bioabsorbable Scaffolds: Magmaris Versus Absorb in a Porcine Arteriovenous Shunt Model. *Circ Cardiovasc Interv.* 2017;10:e004762.

Supplementary data

Supplementary Appendix 1. Quantitative OCT analysis.
Supplementary Appendix 2. Qualitative OCT findings.
Supplementary Appendix 3. Scaffold restenosis types.
Supplementary Figure 1. Case 1 of MgBRS restenosis.
Supplementary Figure 2. Case 2 of MgBRS restenosis.
Supplementary Figure 3. Case 3 of MgBRS restenosis.
Supplementary Figure 4. Case 4 of MgBRS restenosis.
Supplementary Figure 5. Case 5 of MgBRS restenosis.
Supplementary Figure 6. Case 6 of MgBRS restenosis.
Supplementary Figure 7. Case 7 of MgBRS restenosis.
Supplementary Figure 8. Case 8 of MgBRS restenosis.
Supplementary Figure 9. Case 9 of MgBRS restenosis.
Supplementary Figure 10. Case 10 of MgBRS restenosis.
Supplementary Figure 11. Case 11 of MgBRS restenosis.
Supplementary Figure 12. Case 12 of MgBRS restenosis.
Supplementary Table 1. Clinical characteristics of patients with and without OCT (per protocol).
Supplementary Table 2. Procedural characteristics of patients with and without OCT (per protocol).
Supplementary Table 3. Quantitative coronary angiography analysis of patients with and without OCT (per protocol).
Supplementary Table 4. Procedural characteristics of the OCT group (per protocol).
Supplementary Table 5. Description of cases with scaffold restenosis.

The supplementary data are published online at: https://eurointervention.pcronline.com/doi/10.4244/EIJ-D-20-00198

Supplementary data

Supplementary Appendix 1. Quantitative OCT analysis

Quantitative OCT analysis was performed each 1 mm according to standard core laboratory procedures using the specific off-line software (LightLab Imaging, USA). In summary, the software drew the lumen contour automatically of all proximal, scaffold/stent and distal segments. Due to the advanced bioresorption state of the MgBRS at one year, lumen contours were obtained using the proximal and distal radiopaque markers as landmarks of the scaffold edges. For the same reason, scaffold contours were only measured in cases of clearly visible strut footprints (either malapposed, protruding or embedded into the vessel wall) in the entire lumen perimeter. MgBRS contours were drawn on the inner strut surface. The stent contour of permanent SES was obtained semi-automatically by following the inner strut surface of the struts. Due to the different strut thickness of the Orsiro stent (60 μm for nominal stent sizes ≤3 mm and 80 μm for nominal stent sizes >3 mm) and the OCT axial resolution (15 μm), strut malapposition was defined as distances between the inner strut surface and the lumen contour greater than 80 μm (for ≤3 mm stents) and 100 μm (for >3 mm stents).

Supplementary Appendix 2. Qualitative OCT findings

In the case of SES, the following qualitative OCT findings were assessed: the observation of cross-sections with a ratio of uncovered to total stent struts (RUTSS) ≥30%, coronary evaginations, major coronary evaginations and neoatherosclerotic plaques. Due to the heterogeneity of the atherosclerotic plaques behind the struts with contiguous regions presenting with fibrotic, fibrolipidic and fibrocalcific; plaque type behind the struts was defined as the most predominant type throughout the stent length.

Supplementary Appendix 3. Scaffold restenosis types

In-segment MgBRS restenosis was defined as a quantitative coronary angiographic diameter stenosis ≥50%. Mechanisms of in-segment MgBRS restenosis, as assessed by OCT, were categorised as follows: 1) scaffold collapse was defined in cases with scaffold expansion ≤0.5, without evidence of scaffold underexpansion at the end of scaffold implantation procedure (angiographic diameter stenosis <20%); 2) scaffold discontinuities were defined in case of struts overhanging each other at the same angular sector, with or without malapposition, or isolated struts at the luminal centre without an obvious connection to other surrounding struts; 3) excessive neointima was defined in case of maximal neointima area stenosis ≥50%; and finally 4) unknown causes were defined in cases with <40% of cross-sections not suitable for scaffold area measurement.

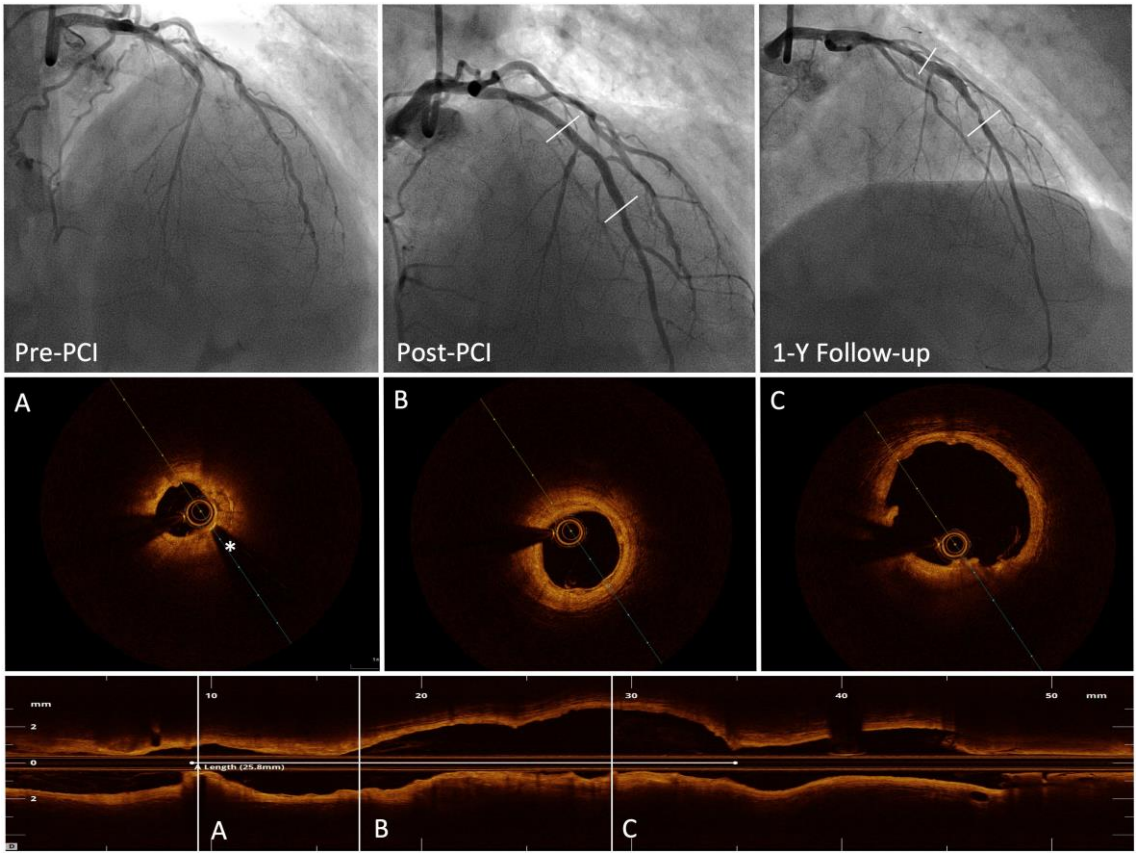

Supplementary Figure 1. Case 1 of MgBRS restenosis.

Main cause of restenosis: scaffold collapse. The OCT images show remnant struts protruding and integrated into the vessel wall with scaffold recoil at the distal edge: scaffold expansion=0.46.
* Distal radiopaque marker

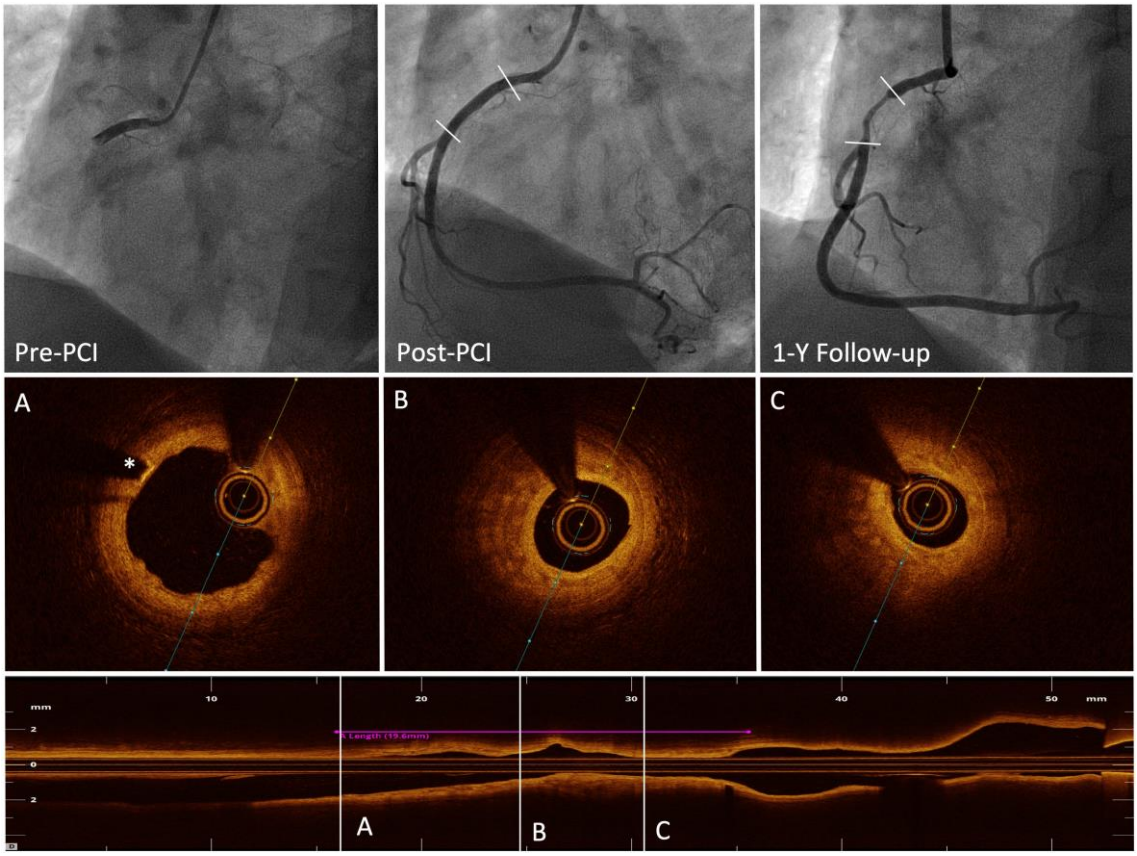

Supplementary Figure 2. Case 2 of MgBRS restenosis.

Causes of restenosis: scaffold collapse+excessive neointima. The OCT images show remnant struts integrated into the vessel wall with scaffold collapse (stent expansion=0.36) and excessive homogeneous neointima tissue (maximal neointima stenosis of 56%).
* Distal radiopaque marker

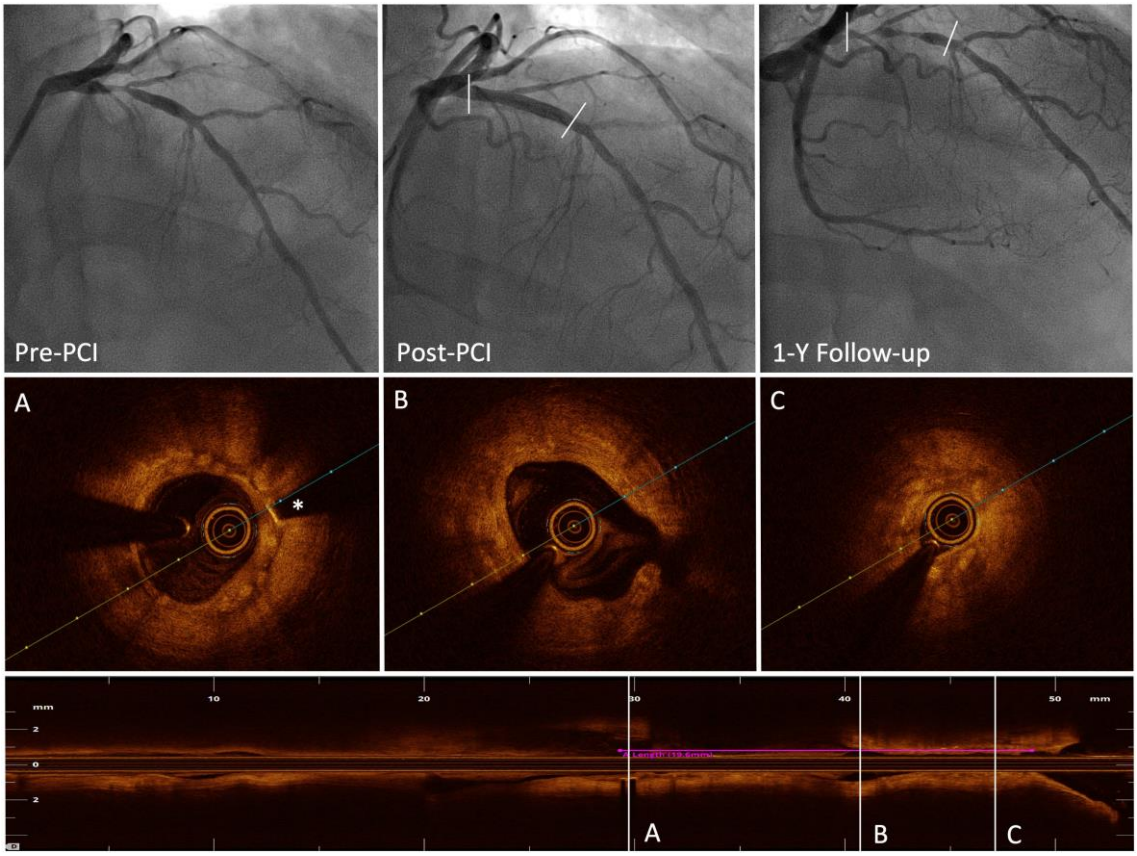

Supplementary Figure 3. Case 3 of MgBRS restenosis.

Cause of restenosis: scaffold collapse. The OCT images show remnant struts integrated into the vessel with scaffold recoil (scaffold expansion=0.13).
* Distal radiopaque marker

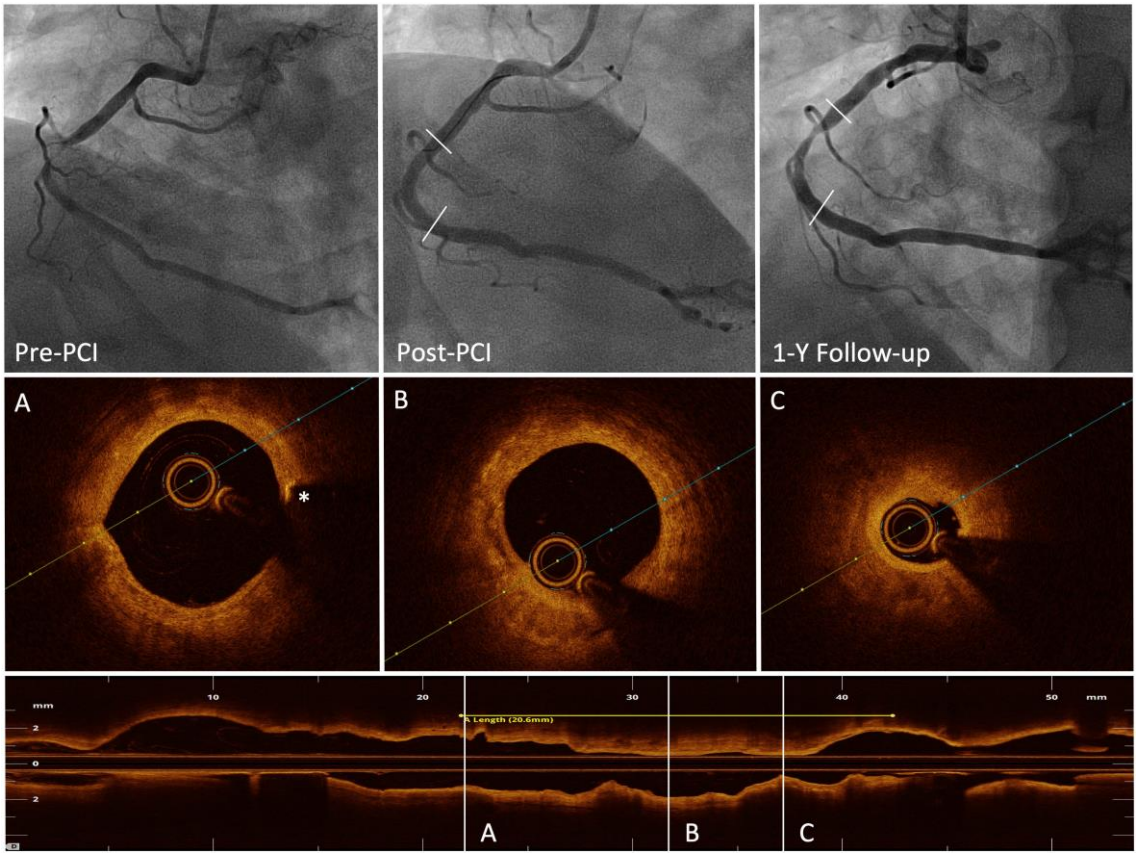

Supplementary Figure 4. Case 4 of MgBRS restenosis.

Cause of restenosis: unknown. The OCT images show indiscernible struts throughout the scaffold segment. The minimal lumen area (1.07 mm^2) cross-section presented an homogeneous neointima layer.
* Distal radiopaque marker

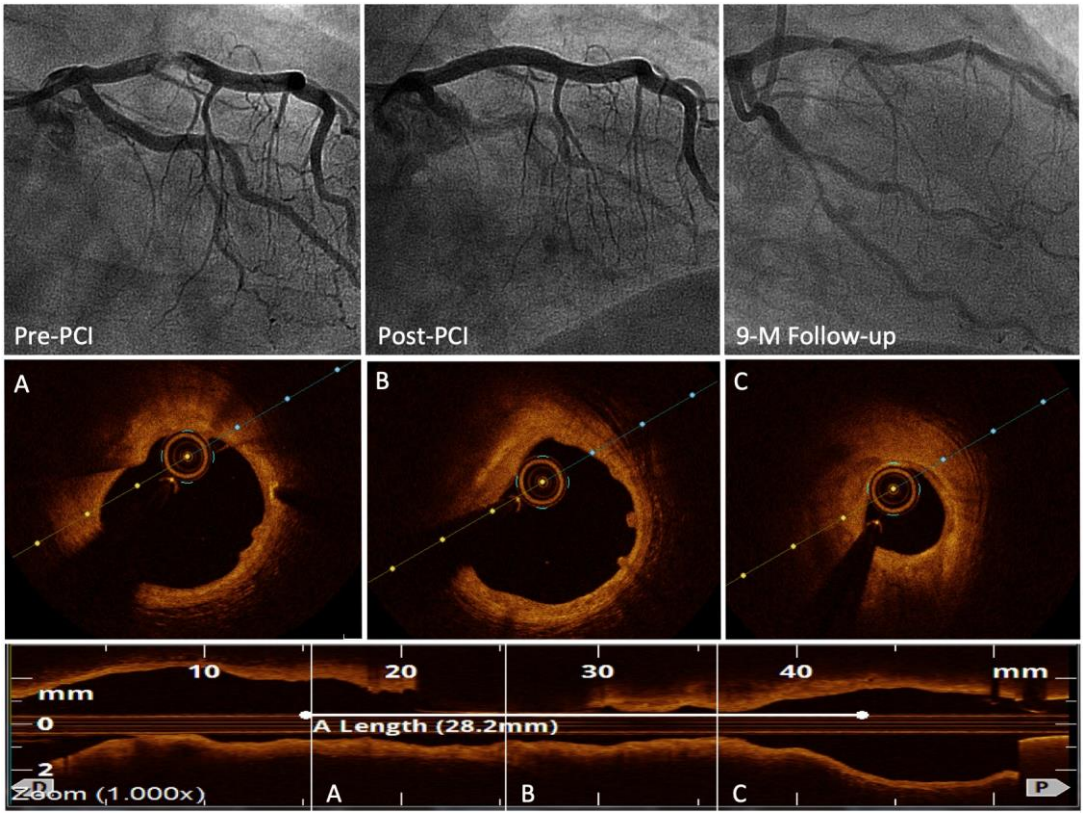

Supplementary Figure 5. Case 5 of MgBRS restenosis.

Cause of restenosis: scaffold collapse. The OCT images show remnant struts protruding into the lumen (distal segment) and struts integrated into the vessel wall (proximal segment) with scaffold collapse (scaffold expansion=0.48).
* Distal radiopaque marker

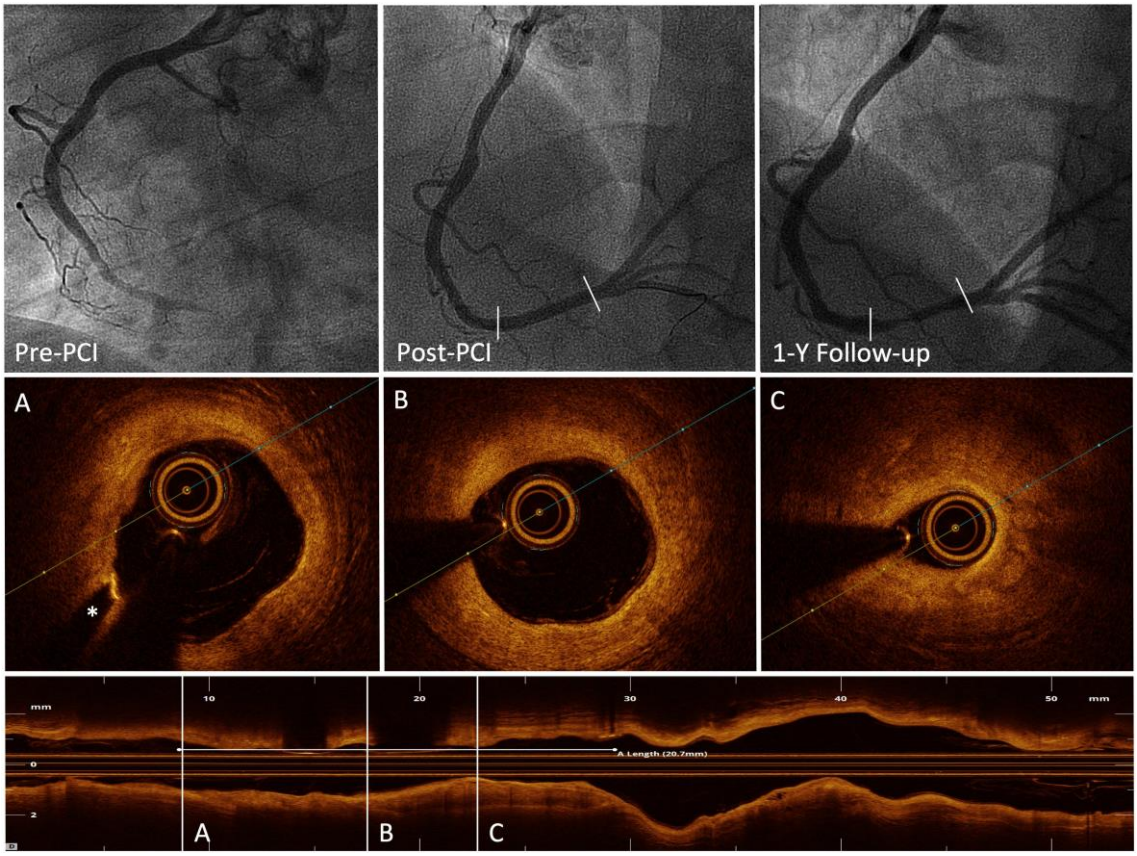

Supplementary Figure 6. Case 6 of MgBRS restenosis.

Cause of restenosis: unknown. The OCT images show indiscernible struts throughout the scaffold segment. The minimal lumen area (0.98 mm^2) cross-section presented an homogeneous neointima layer.
* Distal radiopaque marker

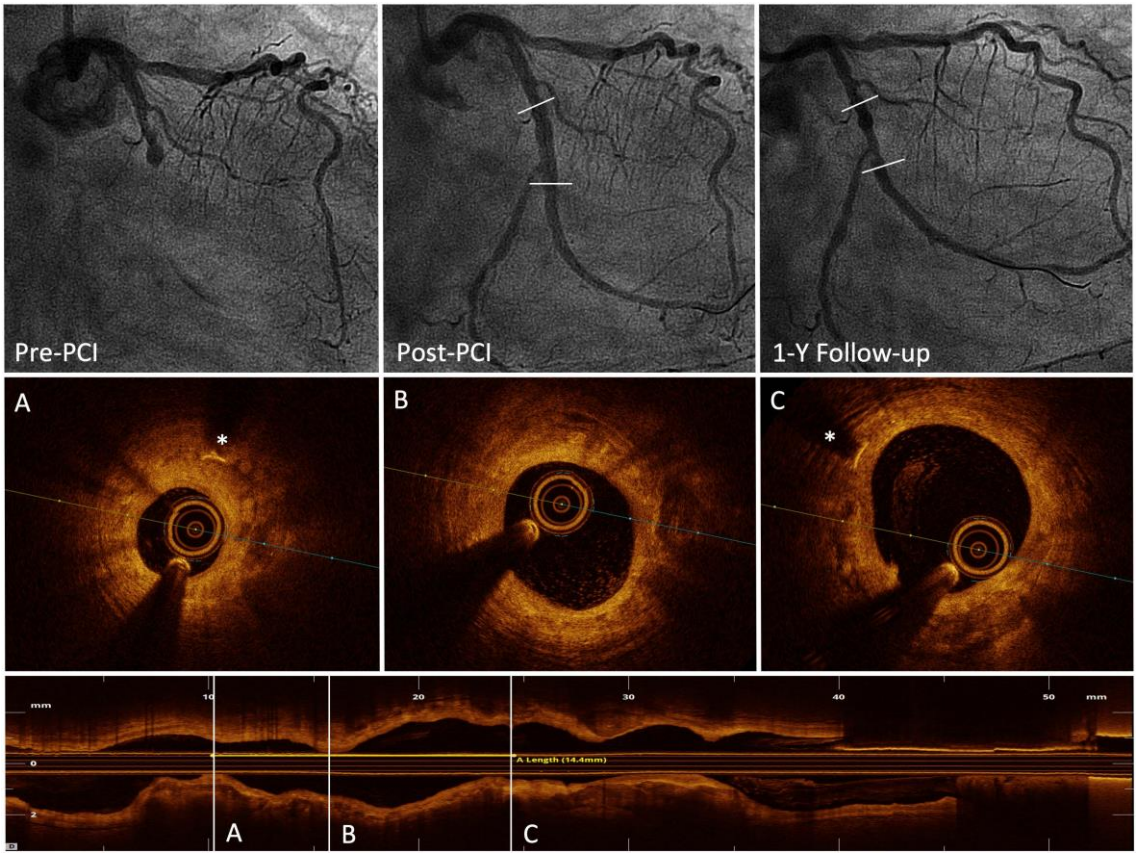

Supplementary Figure 7. Case 7 of MgBRS restenosis.

Cause of restenosis: excessive neointima. The OCT images show remnant struts integrated into the vessel wall throughout the scaffold segment. Excessive homogeneous neointima tissue (maximal neointima stenosis of 52%).
* Distal radiopaque marker

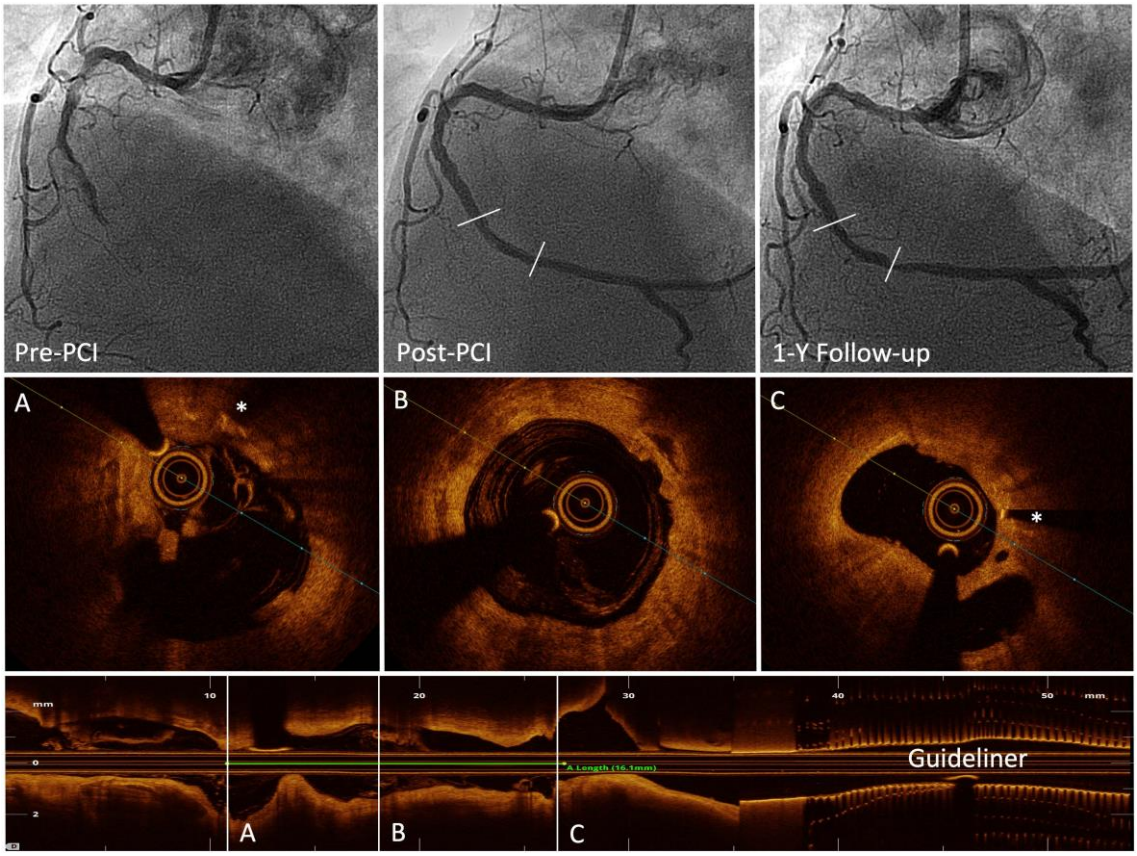

Supplementary Figure 8. Case 8 of MgBRS restenosis.

Cause of restenosis: unknown. The OCT images show remnant fractured struts in the distal scaffold edge and indiscernible struts in mid and proximal segments. The proximal edge presents with focal restenosis (MLA=2.6 mm²) due to unknown cause.
* Distal radiopaque marker

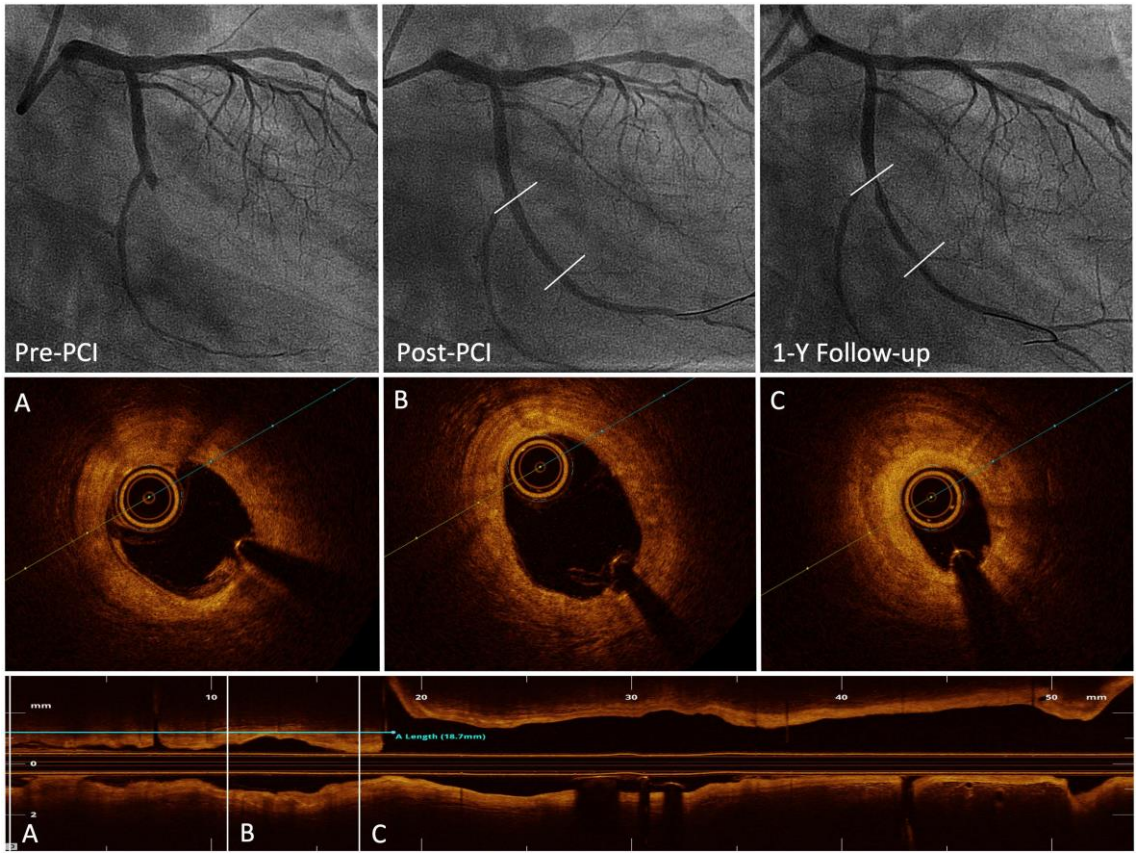

Supplementary Figure 9. Case 9 of MgBRS restenosis.

Cause of restenosis: excessive neointima. The OCT images show remnant struts integrated into the vessel wall throughout the scaffold segment with focal proximal restenosis due to excessive homogeneous neointima tissue (maximal neointima stenosis of 53%).

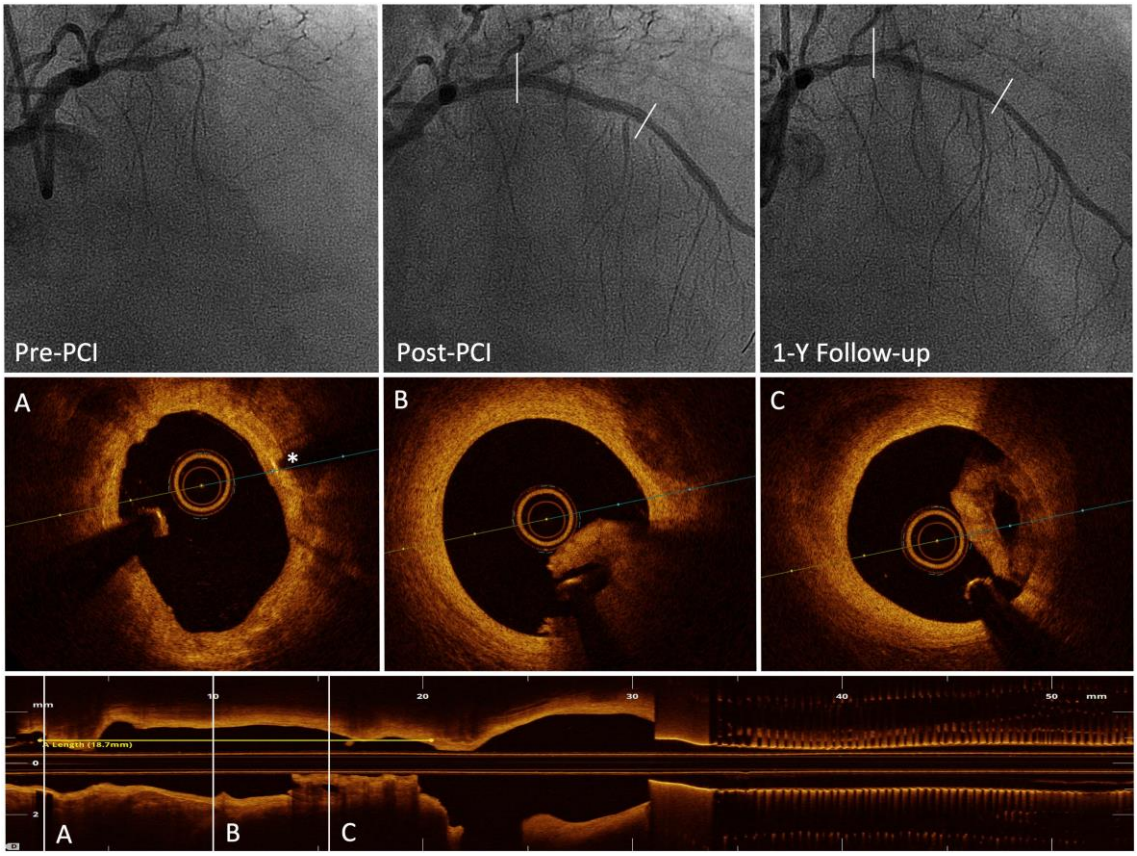

Supplementary Figure 10. Case 10 of MgBRS restenosis.

Cause of restenosis: scaffold discontinuity. The OCT images show probable scaffold fracture during baseline procedure. The intracoronary wire probably re-crossed outside the scaffold before post-dilatation. At follow-up, the scaffold is crushed outside the OCT catheter.
* Distal radiopaque marker

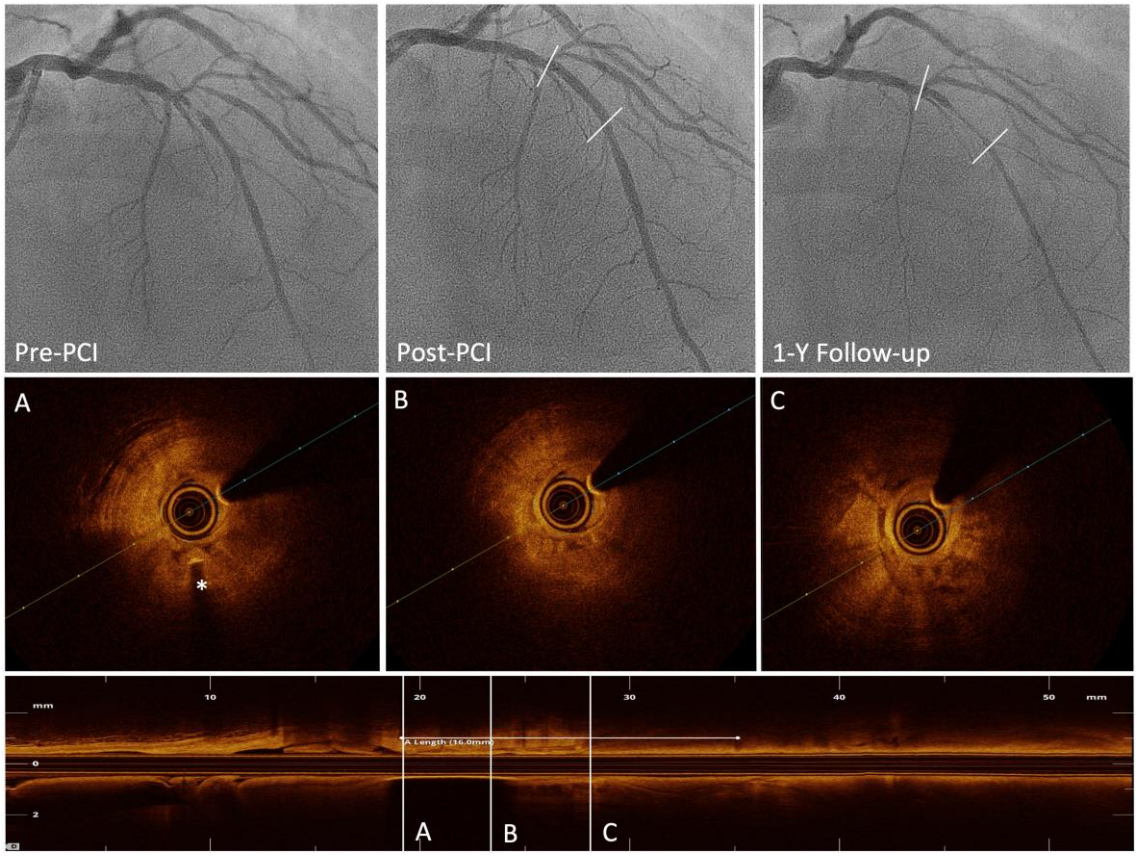

Supplementary Figure 11. Case 11 of MgBRS restenosis.

Cause of restenosis: scaffold collapse. Poor quality OCT imaging due to critical restenosis. However, there are remnant struts throughout the scaffold segment with diffuse scaffold collapse (scaffold expansion=0.29).
* Distal radiopaque marker

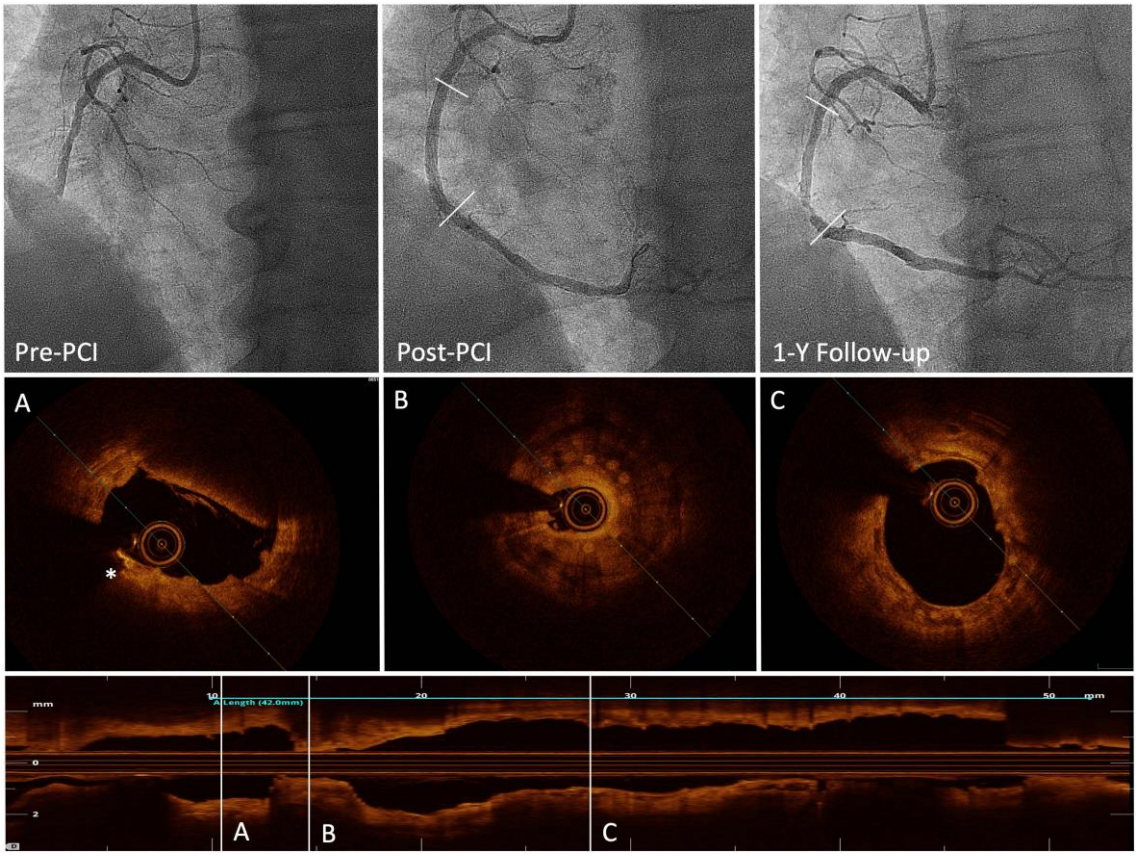

Supplementary Figure 12. Case 12 of MgBRS restenosis.

Cause of restenosis: scaffold collapse. The OCT images show remnant struts integrated into the vessel wall throughout the scaffold segment. Scaffold collapse of the distal segment (scaffold expansion=0.42). Important systo-diastolic movement of the collapsed region as the most plausible explanation of the scaffold collapse.
* Distal radiopaque marker

Supplementary Table 1. Clinical characteristics of patients with and without OCT (per protocol).

	OCT N=97	**No OCT N=37**	***p*-value**
Demographic data			
Age, years, mean (SD)	59.36 (10.05)	56.69 (10.70)	0.181
Males, n (%)	85 (87.6)	35 (94.6)	0.239
Coronary risk factors, n (%)			
Current smoker	55 (56.7)	21 (56.8)	0.403
Diabetes mellitus	19 (19.6)	4 (10.8)	0.228
Insulin-dependent	3 (15.8)	1 (25.0)	1.000
Hypertension	43 (44.3)	15 (40.5)	0.692
Hypercholesterolaemia	59 (60.8)	20 (54.1)	0.476
Family history of coronary artery disease	9 (9.3)	10 (27.0)	0.009
Medical history, n (%)			
Previous myocardial infarction	7 (7.2)	1 (2.7)	0.324
Previous percutaneous coronary intervention	4 (4.1)	1 (2.7)	1.000
Chronic obstructive pulmonary disease	6 (6.2)	0 (0.0)	0.122

MgBRS: magnesium-based bioresorbable scaffold; PCI: percutaneous coronary intervention; SD: standard deviation; SES: sirolimus-eluting stent

Supplementary Table 2. Procedural characteristics of patients with and without OCT (per protocol).

	OCT N=97	No OCT N=37	*p*-value
Pre-procedure specifications			
Killip class			0.489
Class 1	94 (96.9)	34 (94.4)	
Class 2	2 (2.1)	2 (5.6)	
Class 3	1 (1.0)	0 (0.0)	
Chest pain to FMC, min, median (IQR)	75 (30, 150)	60 (32, 150)	0.802
FMC to wiring, min, median (IQR)	94 (69, 124)	94 (75, 142)	0.429
Chest pain to wiring, min, median (IQR)	172 (117, 279)	166 (123, 308)	0.831
Culprit artery			0.543
Left anterior descending	48 (49.5)	16 (43.2)	
Right coronary	30 (30.9)	15 (40.5)	
Circumflex	19 (19.6)	6 (16.3)	
Periprocedural medication			
Aspirin	95 (97.9)	36 (97.3%)	0.624
Heparin	93 (95.9)	35 (94.6%)	0.668
Antiplatelet therapy			0.188
Prasugrel	21 (21.6)	3 (8.1)	
Ticagrelor	45 (46.4)	20 (54.1)	
Clopidogrel	31 (32.0)	14 (37.8)	
Glycoprotein IIb/IIIa antagonists	17 (17.5)	10 (27.0)	0.220
Number of lesions per patient	1.0±0.1	1.2±0.6	0.009
Pre-PCI TIMI flow			0.025
0	73 (73.7)	22 (50.0)	
1	7 (7.1)	3 (6.8)	
2	6 (6.1)	7 (15.9)	
3	13 (13.1)	12 (27.3)	
Lesion preparation			
Thrombectomy attempted	63 (63.6)	26 (59.1)	0.605
Retrieval of visible thrombus	37 (38.5)	16 (37.2)	0.881
Predilation	91 (91.9)	36 (81.8)	0.078
Stent implantation			
Number of stents per lesion	1.0±0.1	1.1±0.1	0.017
Stent length, mm	20.2±5.1	20.7±3.5	0.002
Stent diameter, mm	3.4±0.2	3.3±0.4	0.056
Maximum stent pressure, atm	16.0±2.7	14.7±3.1	0.015
Post-dilation, l (%)	56 (56.6)	24 (54.5)	0.822
Maximum pressure, atm	18.59±3.53	16.54±2.99	0.009
Balloon length, mm	13.52±4.13	13.63±4.19	0.996
Balloon diameter, mm	3.35±0.33	3.44±0.38	0.143

FMC: first medical contact; IQR: interquartile range; l: number of lesions; MgBRS: magnesium-based bioresorbable scaffold; N: number of patients; PCI: percutaneous coronary intervention; SD: standard deviation; SES: sirolimus-eluting stent; TIMI: Thrombolysis In Myocardial Infarction

Supplementary Table 3. Quantitative coronary angiography analysis of patients with and without OCT (per protocol).

Index procedure	OCT N=97	No OCT N=37	*p*-value
Pre-PCI			
MLD, mm	0.19±0.37	0.32±0.47	0.136
%DS	93.01±13.19	88.54±16.02	0.136
Post PCI			
In-stent			
Length, mm	19.08±5.53	20.40±8.94	0.406
Mean LD, mm	2.95±0.35	3.00±0.38	0.489
MLD, mm	2.60±0.37	2.68±0.37	0.267
RVD, mm	2.88±0.40	2.88±0.39	1.000
%DS	9.49±5.52	6.76±5.23	0.010
In-segment			
Length, mm	28.62±5.68	30.00±9.02	0.390
Mean LD, mm	2.89±0.35	2.92±0.40	0.690
MLD, mm	2.19±0.41	2.27±0.52	0.404
RVD, mm	2.75±0.43	2.80±0.46	0.569
%DS	20.39±9.54	19.43±9.63	0.607
In-stent acute gain, mm	2.41±0.55	2.36±0.51	0.621
In-segment acute gain, mm	2.00±0.57	1.95±0.57	0.651
Follow-up	**OCT N=97**	**No OCT N=37**	***p*-value**
In-stent			
Length, mm	19.18±5.62	20.50±8.91	0.405
Mean LD, mm	2.80±0.48	2.86±0.42	0.480
MLD, mm	2.28±0.63	2.33±0.68	0.699
RVD, mm	2.82±0.41	2.79±0.38	0.691
%DS	19.71±16.84	15.88±22.35	0.349
In-segment			
Length, mm	28.79±5.80	30.09±8.98	0.417
Mean LD, mm	2.77±0.42	2.80±0.40	0.703
MLD, mm	2.01±0.52	2.01±0.62	1.000
RVD, mm	2.73±0.44	2.75±0.42	0.809
%DS	26.47±14.35	26.66±20.03	0.958
Late lumen loss			
In-stent LLL, mm	0.32±0.46	0.35±0.59	0.782
In-segment LLL, mm	0.18±0.38	0.27±0.55	0.364
In-stent binary restenosis	10 (10.3)	3 (8.1)	1.000
In-segment binary restenosis	10 (10.3)	4 (10.8)	1.000

Data are presented as mean±standard deviation or n (%).
DS: diameter stenosis; LLL: late lumen loss; Mean LD: mean lumen diameter; MLD: minimal lumen diameter; OCT: optical coherence tomography; PCI: percutaneous coronary intervention; RVD: reference vessel diameter

Supplementary Table 4. Procedural characteristics of the OCT group (per protocol).

	MgBRS N=50	**SES N=47**	***p*-value**
Killip class, n (%)			1.000
Class 1	48 (96.0)	46 (97.9)	
Class 2	1 (2.0)	1 (2.1)	
Class 3	1 (2.0)	0 (0.0)	
Chest pain to FMC, min, median (IQR)	48 (30, 120)	80 (34, 160)	0.183
FMC to wiring, min, median (IQR)	94 (62, 120)	98 (75, 124)	0.307
Chest pain to wiring, min, median (IQR)	160 (113, 271)	210 (128, 279)	0.301
Culprit artery, n (%)			0.687
Left anterior descending	25 (50.0)	23 (48.9)	
Right coronary	13 (26.0)	17 (36.2)	
Circumflex	12 (24.0)	7 (14.9)	
Periprocedural medication, n (%)			
Aspirin	49 (98.0)	46 (97.9)	0.737
Heparin	48 (96.0)	45 (95.7)	1.000
Antiplatelet therapy			0.378
Prasugrel	8 (16.0)	13 (27.7)	
Ticagrelor	25 (50.0)	20 (42.6)	
Clopidogrel	17 (34.0)	14 (29.8)	
Glycoprotein IIb/IIIa antagonists	8 (16.0)	9 (19.1)	0.683
Number of lesions per patient	1.01±0.1	1.02±0.1	0.979
Pre-PCI TIMI flow, n (%)			1.000
Flow 0	37 (72.5)	36 (75.0)	
Flow 1	4 (7.8)	3 (6.3)	
Flow 2	3 (5.9)	3 (6.3)	
Flow 3	7 (13.7)	6 (12.5)	
Lesion preparation			
Thrombectomy attempted, n (%)	32 (62.7)	31 (64.6)	0.849
Predilation, n (%)	49 (96.1)	42 (87.5)	0.117
Maximum pressure, atm	15.0±2.9	14.7±2.2	0.835
Balloon length, mm	12.5±3.6	12.2±2.7	0.741
Balloon diameter, mm	2.6±0.45	2.6±0.4	0.593
Stent implantation			
Number of stents	1.0±0.0	1.1±0.1	0.989
Stent length, mm	20.7±3.8	19.7±6.1	0.207
Stent diameter, mm	3.3±0.3	3.5±0.2	0.086
Maximum stent pressure, atm	15.4±2.4	16.6±2.8	0.029
Post-dilation, n (%)	48 (94.1)	8 (16.7)	0.001
Maximum pressure, atm	18.5±3.1	19.0±5.5	0.701
Balloon length, mm	13.8±4.3	11.8±2.7	0.216
Balloon diameter, mm	3.5±0.0	3.4±0.3	0.080
Non-compliant balloon, n (%)	44 (93.6)	8 (100.0)	1.000
Post-PCI TIMI flow, n (%)			
2	0 (0.0)	0 (0.0)	
3	51 (100.0)	48 (100.0)	

Data are presented as mean±standard deviation or n (%).
FMC: first medical contact; IQR: interquartile range; PCI: percutaneous coronary intervention; TIMI: Thrombolysis In Myocardial Infarction

Supplementary Table 5. Description of cases with scaffold restenosis.

n	Device	Artery	Event	Clinical presentation	Main cause	OCT findings
1	Magmaris 3.0x25 mm	Mid LAD (RVD=2.46 mm)	ID-TLR	Asymptomatic at 1 year. Angiographic focal distal restenosis (DS=51%) at 1 year. FFR <0.80. Treated with PCI.	Scaffold collapse	Remnant struts protruding and integrated into the vessel wall. Scaffold recoil at distal edge (SE=0.46). Supplementary Figure 1
2	Magmaris 3.0x20 mm	Proximal RCA (RVD=2.63 mm)	No event (angio. restenosis)	Asymptomatic at 1 year. Angiographic diffuse restenosis (DS=57%) at 1 year. FFR >0.80. Optimal medical therapy.	Scaffold collapse + excessive neointima	Predominant remnant struts integrated into the vessel wall. Scaffold collapse (SE=0.36)+excessive homogeneous neointima tissue (maximal neointima stenosis of 56%). Supplementary Figure 2
3	Magmaris 3.5x20 mm	Proximal LAD (RVD=3.09 mm)	ID-TLR	Asymptomatic at 1 year. Critical diffuse angiographic restenosis (DS=76%) at 1 year. No FFR. Treated with PCI.	Scaffold collapse	Remnant struts integrated into the vessel wall. Focal scaffold collapse (SE=0.13). Supplementary Figure 3
4	Magmaris 3.0x20 mm	Mid RCA (RVD=3.07 mm)	ID-TLR	Asymptomatic at 1 year. Angiographic focal restenosis (DS=72%) at 1 year. FFR <0.80. Treated with PCI.	Unknown	Predominant indiscernible struts. The minimal lumen area (1.07 mm^2) cross-section had homogeneous neointima. Supplementary Figure 4
5	Magmaris 3.5x20 mm	Proximal LAD (RVD=3.33 mm)	ID-TLR	Stable angina. Underwent clinically indicated coronariography at 9 months. Focal restenosis (DS=64%). Treated with PCI.	Scaffold collapse	Remnant struts protruding into the lumen (dist. segment). Struts integrated into the vessel wall (prox. segment) with scaffold collapse (SE=0.48). Supplementary Figure 5
6	Magmaris 3.0x20 mm	Distal RCA (RVD=2.85 mm)	ID-TLR	Asymptomatic at 1 year. Angiographic focal restenosis (DS=55%) at 1 year. FFR <0.80. Treated with PCI.	Unknown	Predominant indiscernible struts. The narrowest cross-section (0.98 mm^2) presented homogeneous neointima. Supplementary Figure 6
7	Magmaris 3.0x15 mm	Mid LCF (RVD=2.35 mm)	No event (angio. restenosis)	Asymptomatic at 1 year. Angiographic distal focal restenosis (DS=55%) at 1 year. FFR >0.80. Optimal medical therapy.	Excessive neointima	Predominant remnant struts integrated into the vessel wall. Excessive homogeneous neointima tissue (maximal neointima stenosis of 52%). Supplementary Figure 7
8	Magmaris 3.0x20 mm	Mid RCA (RVD=2.49 mm)	No event (angio. restenosis)	Asymptomatic at 1 year. Angiographic proximal focal restenosis (DS=50%) at 1 year. FFR >0.80. Optimal medical therapy.	Unknown	Remnant fractured struts in the distal scaffold edge and indiscernible struts in mid and proximal segments. Proximal focal restenosis (MLA=2.6 mm^2) due to unknown cause. Supplementary Figure 8

9	Magmaris 3.5x25 mm	Mid LCF (RVD=2.17 mm)	ID-TLR	Asymptomatic at 1 year. Angiographic proximal focal restenosis (DS=61%) at 1 year. FFR<0.80. Underwent PCI.	Excessive neointima	Predominant remnant struts integrated into the vessel wall. Focal restenosis due to excessive homogeneous neointima (maximal neointima stenosis of 53%). Supplementary Figure 9
10	Magmaris 3.0x25 mm	Proximal LAD (RVD=2.57 mm)	ID-TLR	Asymptomatic at 1 year. Angiographic proximal focal restenosis (DS=51%) at 1 year. Underwent PCI.	Scaffold discontinuity	Probable scaffold fracture during baseline procedure. The intracoronary wire probably re-crossed outside the scaffold before post-dilatation. At 1 year, the scaffold is crushed outside the OCT catheter. Supplementary Figure 10
11	Magmaris 3.0x20 mm	Mid LAD (RVD=2.89 mm)	ID-TLR	Asymptomatic at 1 year. Angiographic diffuse severe restenosis (DS=79%) at 1 year. Underwent PCI.	Scaffold collapse	Poor quality imaging due to critical restenosis. Diffuse scaffold recoil (SE=0.29). Supplementary Figure 11
12	Magmaris 3.5x25 mm+ 3.5x20 mm	Mid RCA (RVD=3.05 mm)	ID-TLR	Asymptomatic at 1 year. Angiographic diffuse in-scaffold restenosis (DS=75%) at 1 year. Underwent PCI.	Scaffold collapse	Predominant remnant struts integrated into the vessel wall. Scaffold collapse of the distal segment (SE=0.42). Important systo-diastolic movement of the collapsed region as most plausible explanation. Supplementary Figure 12
13	Magmaris 3.0x15 mm	Distal LAD (RVD=2.43 mm)	ID-TLR	Asymptomatic at 1 year. In-segment distal restenosis at 1 year. Treated with PCI.	Probable geographical miss at baseline	No OCT imaging
14	Magmaris 3.5x20 mm	Mid LAD (RVD=2.91 mm)	No event (angio. restenosis)	Asymptomatic at 1 year. Complete total occlusion of the scaffold segment at 1 year. Planned elective PCI.	Unknown	No OCT imaging

DS: diameter stenosis; FFR: fractional flow reserve; ID-TLR: ischaemia-driven target lesion revascularisation; LAD: left anterior descending; LCF: left circumflex; RCA: right coronary artery; RVD: reference vessel diameter; SE: scaffold expansion